*Economic Geology*
Vol. 90, 1995, pp. 616–635

# A Review of the Geology, Mineralization, and Geochronology of the Greenbushes Pegmatite, Western Australia

G.A. PARTINGTON*, N.J. MCNAUGHTON,

*Key Centre for Strategic Mineral Deposits, Department of Geology and Geophysics, University of Western Australia, Nedlands, Western Australia 6907, Australia*

AND I.S. WILLIAMS

*Research School of Earth Sciences, Australian National University, G.P.O. Box 4, Canberra, ACT 2601, Australia*

## Abstract

The Greenbushes pegmatite is a giant pegmatite dike of Archean age with substantial Li-Sn-Ta mineralization, including half the world's Ta resource. The pegmatite was intruded and crystallized synchronously with deformation and has a medium- to high-temperature and medium-pressure metamorphic setting. Four major compositional zones and four subsidiary zones have been recognized in the pegmatite. This zonation is unusual, and perhaps unique, in that those zones expected to crystallize last and in the center of the pegmatite (e.g., lithium zones) occur as footwall and hanging-wall marginal zones. Ore mineralogical studies have identified more than ten Ta-bearing phases; cassiterite is the main Sn-bearing phase and spodumene the main Li-bearing phase. The main ore shoots occur exclusively in the albite zones in the pegmatite and generally within tourmaline-rich subzones. Tin and tantalum mineralization appear to have crystallized synchronously with tourmaline in both these zones. The lithium ore zones comprise mainly spodumene, apatite, and quartz, with some ore zones returning upward of 5 percent $Li_2O$.

Geochronological studies utilizing imprecise whole-rock Pb-Pb and precise U-Pb zircon techniques on granitoids within the same major shear zone as the pegmatite date the intrusion of the granitoids to about 90 m.y. before the intrusion of the pegmatite; the granitoids have been postulated as the source for the pegmatite. It is therefore unlikely that the pegmatite is genetically related to these granitoids, which show few mineralogically and geochemically characteristics of specialized granitoids. Three mineralizing events are recognized in the pegmatite. The first is related to initial crystallization of the pegmatite and metasomatism of the country rocks (at 2527 Ma). Later or continuing synkinematic and synmetamorphic hydrothermal alteration of the pegmatite produced a second mineralizing event (at ca. 2430 Ma), and finally remobilization of mineralization occurred during later deformation and metamorphism (at ca. 1100 Ma).

## Introduction

THE giant Greenbushes pegmatite is located 250 km south of Perth within the Balingup metamorphic belt (Fig. 1A). Tin and tantalum have been mined from the pegmatite since early 1888, and more recently, mining has yielded lithium and kaolin resources. Present mining reserves stand at $7.1 \times 10^6$ t at 4.06 percent $Li_2O$, $4.7 \times 10^6$ t at 0.06 percent Ta, $10.8 \times 10^6$ t at 0.42 percent Nb, $4.7 \times 10^6$ t at 0.24 percent Sn, and $2.3 \times 10^6$ t at 30 percent kaolin (SOG, 1991). To date, most of the ore has been produced from the weathered pegmatite and alluvial sources. A new deep hard-rock open cut has been commissioned, which has added considerably to the tin and tantalum reserves of the Greenbushes mine. Because of the renewed activity in the hard-rock resource it was considered that a review of the geology of the pegmatite, with an emphasis on the timing of events, was appropriate.

Previous investigations (Koon, 1973; Hartley, 1982; Paterson, 1983; Bettenay et al., 1985, 1988; Partington, 1986, 1988, 1990a and b; Partington et al., 1986; Han, 1991; Han and Collins, 1993), which included structural, mineralogical, isotopic, and fluid inclusion studies, suggested that the pegmatite is unique in comparison to other major rare metal pegmatites. For example, intrusion and crystallization of the pegmatite is synchronous with deformation, the pegmatite has a medium- to high-temperature and medium-pressure metamorphic setting, and it has an apparent reverse internal zoning and unusual ore element distributions. These features have all been explained to some degree by the synmetamorphic and syntectonic emplacement and crystallization of the pegmatite (Partington, 1988, 1990a).

There is no clear chemical and/or mineralogical relationship between the pegmatite and nearby granitoids, as is normally the case with pegmatites (e.g., Černý, 1982a and b). However, there is a spatial relationship between granitoid intrusions and the Greenbushes pegmatite, and a more fractionated apophysis from these granitoids at depth has been invoked as a source for the pegmatite (Blockley, 1980). An integrated study of precise geochronology on granitoids with known structural affinities in the vicinity of the Greenbushes pegmatite was therefore considered important if the source of the pegmatite was to be identified. To this end, detailed structural mapping combined with whole-rock Pb-Pb geochronology and sensitive high-resolution ion microprobe (SHRIMP) U-Pb analyses of zircons were used to decipher the complex geologic history of the district, the timing of the intrusion of the pegmatite, and mineralizing events.

This paper will therefore review the current geologic knowledge, concentrating on the paragenesis and timing of rare element mineralization in the pegmatite, and present

* Present address: Northern Gold, Regional Exploration Office, c/o P.O. Adelaide River, Northern Territory 0846, Australia.

0361-0128/95/1694/616-20$4.00

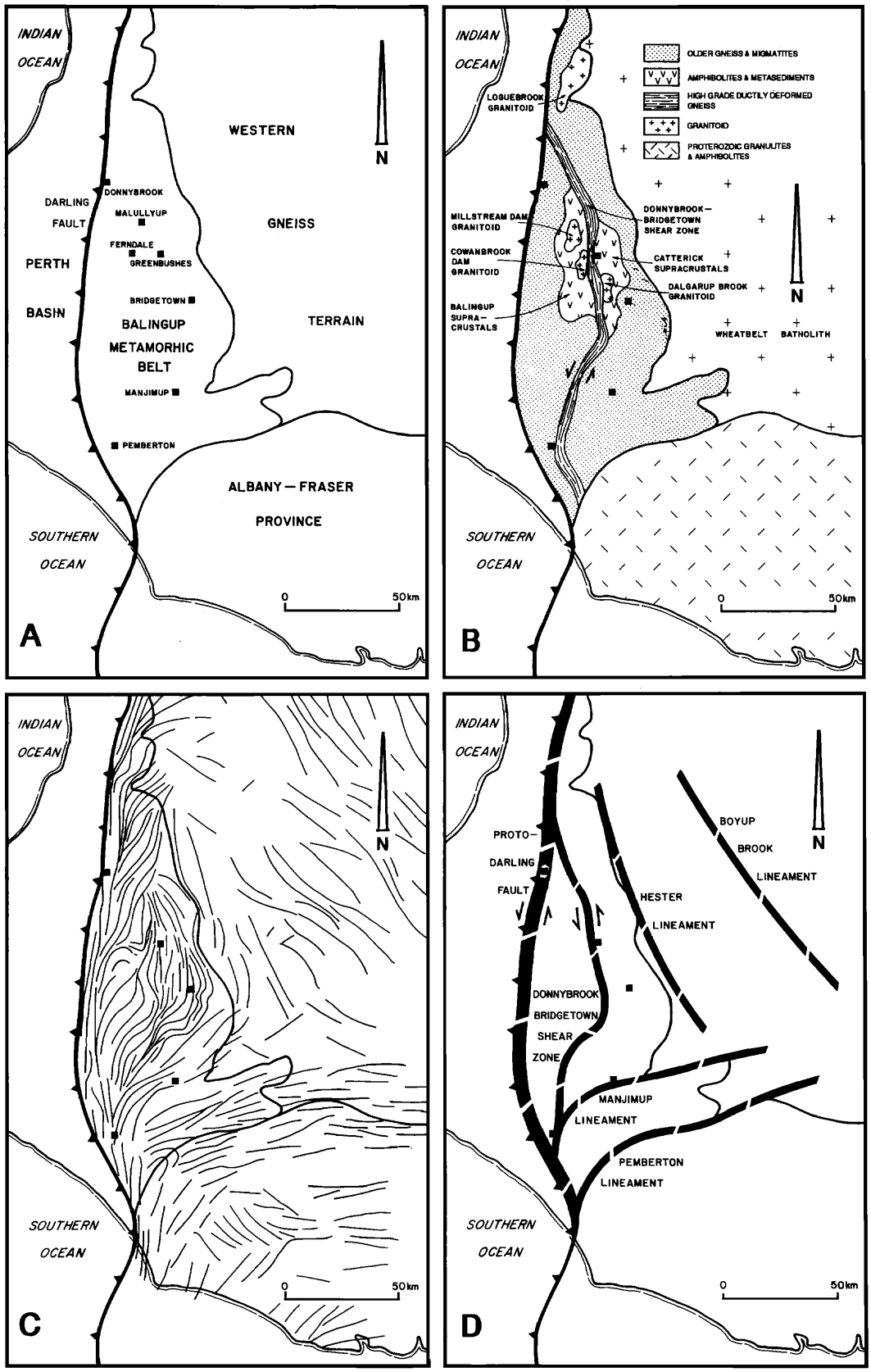


FIG. 1. A. Location of the main geologic terranes. B. Regional geology of the Balingup metamorphic belt. C. Regional foliation trajectory map. D. Regional lineament map. Geochronological samples were taken from the Greenbushes pegmatite, the Millstream Dam granitoid, and the Cowan Brook Dam granitoid (after Partington, 1990a).

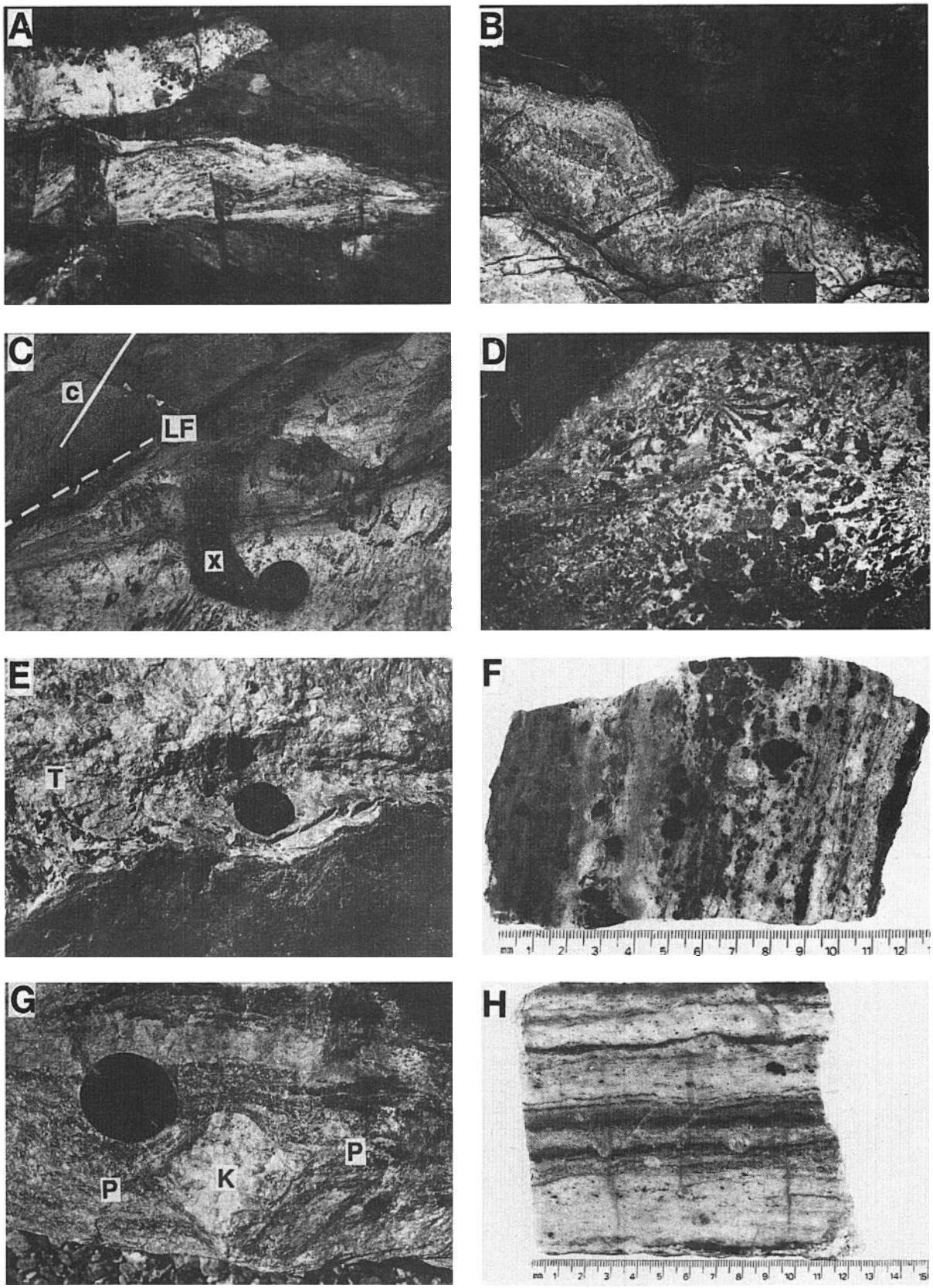
A
B
C
c
LF
X
D
E
T
F
G
P
K
P
H

previously unpublished geochronological results from the pegmatite and spatially related granitoids. These results will be used to reassess the muscovite model Rb-Sr age for the pegmatite of 2650 Ma (de Laeter and Blockley, 1978), and the implications of these results will be discussed with regard to the possible source of the pegmatite. A possible temporal framework for the intrusion, crystallization, and mineralization history of the pegmatite will be proposed, incorporating the fluid inclusion data of Han (1991) and Han and Collins (1993).

## Regional Geology

The Greenbushes pegmatite intrudes rocks of the Balingup metamorphic belt (Fig. 1A), which is one of the four major high-grade gneiss and schist belts recognized in the Archean western gneiss terrane (Gee et al., 1981). The Greenbushes pegmatite district is centered on the Greenbushes mineral field, which includes two major pegmatite groups at Ferndale and Greenbushes, respectively (Fig. 1A). The Greenbushes pegmatite occurs within a 15- to 20-km-wide, north- to northwest-trending regional lineament (Donnybrook-Bridgetown shear zone), which has a strike length of approximately 150 km (Fig. 1B and D). The lineament is subparallel to the Darling fault in the north of the Balingup metamorphic belt and trends northwest to southeast, oblique to the Darling fault, to the south (Fig. 1D).

The main rock types in the pegmatite district include dioritic gneiss, which appears to be basement to Archean greenstonelike sequences of fine-grained amphibolite and associated banded iron-formation, ultramafic schist, coarse-grained amphibolite, and felsic massive to banded paragneiss (Fig. 1B), which are termed "granofels" by the Geological Survey of Western Australia (Wilde and Walker, 1979).

The supracrustal lithologies have been intruded by quartz-biotite-feldspar porphyry dikes, dolerite sills, dolerite dikes and granitoids, which predate the intrusion of the mineralized pegmatites at Greenbushes, and barren pegmatites and dolerite dikes, which postdate intrusion. The later dolerite dikes are oriented east-west, and where they cut the Greenbushes pegmatite, are reintruded by pegmatite veins. These veins are interpreted to have formed due to remelting of the pegmatite at the time of dolerite intrusion (Bettenay et al., 1985).

The granitoid rocks in the Greenbushes pegmatite district can be subdivided on the basis of field relations and geochronology into an older suite, which predates the pegmatites at Greenbushes, and a younger suite which appears to be synchronous with intrusion of the mineralized pegmatites (Partington, 1988, 1990b). The younger granitoids are aligned parallel to the Donnybrook-Bridgetown shear zone and are associated with linear belts of migmatite, and they are believed to form part of the Wheatbelt batholith (Wilde and Walker, 1979; Fig. 1B). Mesoscopic and macroscopic relationships suggest that the younger granitoids and the pegmatites at Greenbushes were intruded synchronously with movements along the Donnybrook-Bridgetown shear zone (Partington, 1988, 1990b). The Logue Brook granitoid (Fig. 1B), which is part of the suite of younger granitoids and is locally deformed by both the proto-Darling fault zone and the Donnybrook-Bridgetown shear zone, has been dated by Compston et al. (1986) at 2612 ± 5 Ma (SHRIMP U-Pb zircon age). The Cowan Brook Dam and Millstream Dam granitoids (Fig. 1B) intruded into $D_2$ shears. The second generation of pegmatites in the Greenbushes mineral field includes the Late Proterozoic Ferndale and Mullalyup pegmatites, which are only weakly mineralized. These pegmatites were intruded during Proterozoic reactivations along the Donnybrook-Bridgetown shear zone, which was accompanied by amphibolite facies metamorphism (Kepert, 1985; Seet, 1986).

Four phases of noncoaxial deformation have been recognized in the pegmatite district, resulting from movements along the Donnybrook-Bridgetown shear zone (Partington, 1988, 1990b). Fabric and structural analyses suggest that $D_1$ predates pegmatite intrusion, $D_2$ predates but is also synchronous with pegmatite intrusion and crystallization, $D_3$ postdates pegmatite intrusion but predates intrusion of the east-west dolerite dikes that cut the Greenbushes pegmatite, and $D_4$ postdates east-west dolerite dike intrusion. The structures associated with these deformation events and their relationship to pegmatite intrusion are described in more detail in Partington (1988, 1990a and b). The metamorphic history of the district is complex with structural and geochronological evidence for four metamorphic episodes closely associated with the deformation events. $M_2$ metamorphism occurs synchronously with $D_2$ deformation and hence provides evidence for the environment of intrusion of the Greenbushes pegmatite (Partington, 1988, 1990a and b). The $M_1$ and $M_3$ metamorphic events pre- and postdate pegmatite intrusion, and the $M_4$ event postdates the intrusion of the east-west dolerite dikes, which have been metamorphosed to hornblende-epidote-biotite assemblages within $D_4$ shear zones.

FIG. 2. Photographs of the Greenbushes pegmatite. A. Two pods of pegmatite (light colored) from the 1160 level of the underground mine (12,900 m N 9,800 m E), initially intruded into a $D_2$ shear zone, which was then deformed by subsequent movements. Field of view = approx 20 m wide. B. Line rock parallel to the irregular contact of the Greenbushes pegmatite from the 1160 level of the mine. Field of view = approx 3 m wide. C. Contact of the pegmatite with mafic country rocks from the Highway shoot area (Fig. 3: 12,900 m N 9,800 m E). Note the $D_2$ fabric (c) cut by the pegmatite, the foliation parallel to the contact (LF), and the xenolith of country rock (x) at the pegmatite margin. Camera cap = 5 cm in diam. D. Undeformed pegmatite with radial tourmalines from the 1160 level of the Greenbushes mine. Field of view = approx 4 m wide. E. Tourmalines (in particular the curved dark crystal directly below T), initially perpendicular to the pegmatite contact, now dragged parallel to the contact as a result of sinistral shear movement along the contact from the 1160 level of the underground mine (12,900 m N 9,800 m E). Camera cap = 5 cm in diam. F. Moderately deformed pegmatite, from the 1160 level of the underground mine (12,900 m N 9,800 m E), with tourmalines beginning to fragment and be drawn out along shear planes. G. Asymmetric pressure shadows (P) in the lee of a K feldspar megacryst (K) indicating sinistral shear movement from the 1160 level of the underground mine (12,900 m N 9,800 m E). Camera cap = 5 cm in diam. H. Hand specimen of highly deformed pegmatite, from the 1160 level of the underground mine (12,900 m N 9,800 m E), in which grain size reduction by fragmentation of brittle minerals and recrystallization is most intense (compare with undeformed pegmatite (D).

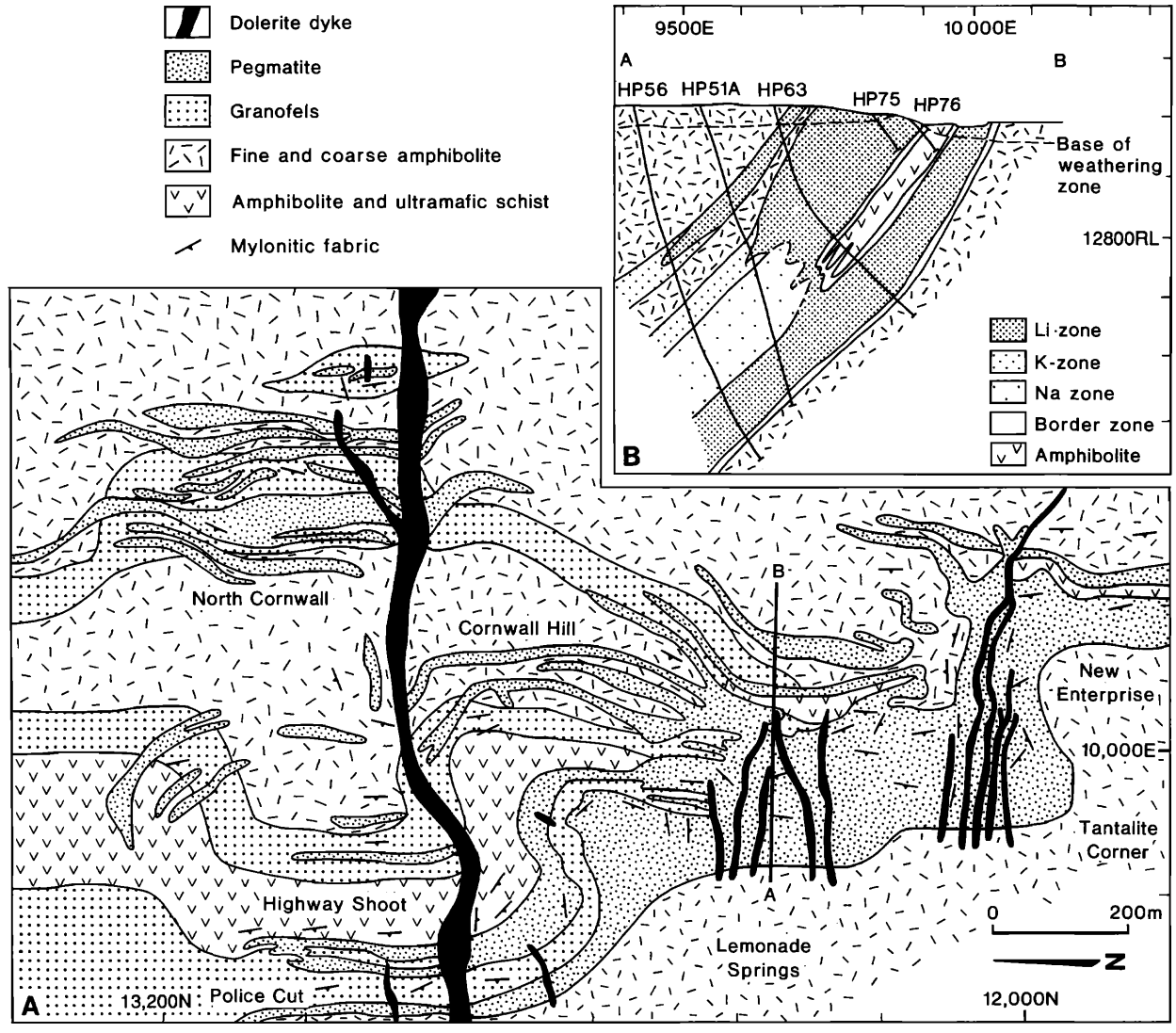


FIG. 3. Geologic map of the Greenbushes pegmatite (A) with a cross section (B) showing the zonation in the pegmatite (after Partington, 1990a).

Temperatures and pressures attained during the various tectonic events were estimated from coexisting minerals within the various structural fabrics. The temperature estimates for the first three metamorphic events in the pegmatite district were in the vicinity of 550° to 650°C (Partington, 1988, 1990a and b). Additional constraints on the temperature of mineral growth for the second tectonic event were derived from the presence of spodumene in the pegmatite (Partington, 1990a) and fluid inclusion studies by Han (1991). Pressures of greater than 4 and up to 5 kbars for the first three metamorphic events are suggested by the presence of almandine garnet and further constrained for the $M_2$ event by staurolite-kyanite assemblages (Partington, 1988, 1990a and b).

## The Greenbushes Pegmatite

### *Distribution and zonation*

The Greenbushes pegmatite was intruded as a series of linear dikes, varying from hundreds of meters to kilometers in length and from tens to hundreds of meters in thickness, to individual pods of a few meters across (Figs. 2A and 3). The pegmatite dikes and en echelon pods are clustered around an intrusive center, which is located within a $D_2$ high strain zone at the boundary between amphibolite and granofels units in the mine sequence (Fig. 3; Partington, 1986, 1988, 1990a and b; Bettenay et al., 1988). Primary features in the pegmatite have been modified to varying degrees by later $D_2$-$D_3$ deformation and $M_2$-$M_4$ metamorphism (Fig. 2; Partington, 1986, 1988, 1990a and b; Bettenay et al., 1988). However, because deformation and metamorphism are heterogeneous, some areas retain primary features such as primary zonation, original fluid inclusions, xenoliths, magmatic layering, and tourmaline rosettes and suns (Fig. 2B and D), whereas other areas are completely recrystallized and sheared, forming classic mylonitic textures (Fig. 2F and H).

The macroscopic zoning in the main pegmatite is largely independent of intercalations of country rock, and because a three-dimensional continuity to the zonal pattern is present

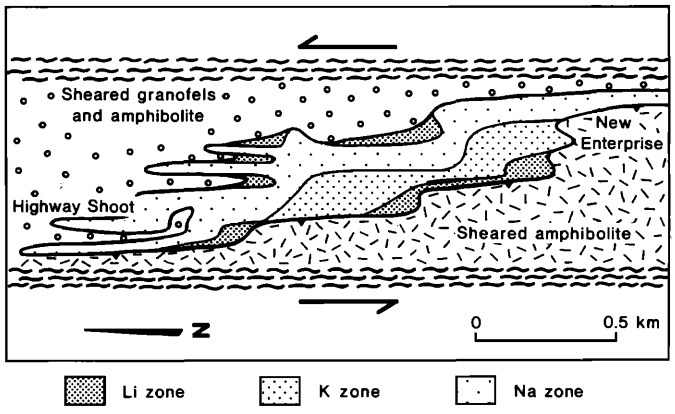


FIG. 4. Schematic plan of the zoning in the Greenbushes pegmatite.

in less deformed areas (Figs. 3 and 4), crystallization from one evolving pegmatite magma is suggested rather than a series of separately emplaced tectonic sheets. Four major and four subsidiary compositional zones have been recognized by various workers in the less deformed portions of the Greenbushes pegmatite (Figs. 3, 4, and 5; Paterson, 1983; Partington, 1986, 1988, 1990a and b; Bettenay et al., 1988; Han, 1991). The main minerals in each zone and their paragenesis are summarized in Figure 5.

Drilling to date, combined with pit mapping, indicates that the northern part of the pegmatite is dominated by subsidiary pods and dikes that are largely monomineralic. There is a general dominance of albite over K feldspar in these pegmatites, which is complemented by a decrease in Li, an increase in Sn and Ta, and an increase in K/Rb, Sr/Rb, K/Li, and Nb/Ta ratios. The main pegmatite in the south is characterized by an outer lithium zone that occurs both in the footwall and hanging wall, the asymmetric development of a K feldspar zone in the hanging wall that decreases in thickness northward, and an albite zone in the footwall of the intrusion (Figs. 3 and 4). The hanging-wall lithium zone also decreases in thickness northward, and eventually disappears completely from the hanging wall.

The contact zones in the undeformed parts of the pegmatite are remarkably similar containing albite, quartz, biotite, tourmaline, holmquistite, tin with tantalite inclusions, garnet, zircon, calcite, and scapolite (Fig. 6A and E). The minerals from this zone appear to be the earliest to have crystallized. The contact zone is usually aplitic, with a granular texture and all but the most resistant minerals annealed. Biotite, scapolite, muscovite, tourmaline, and holmquistite also occur within the metasomatized exocontact zone of the pegmatite

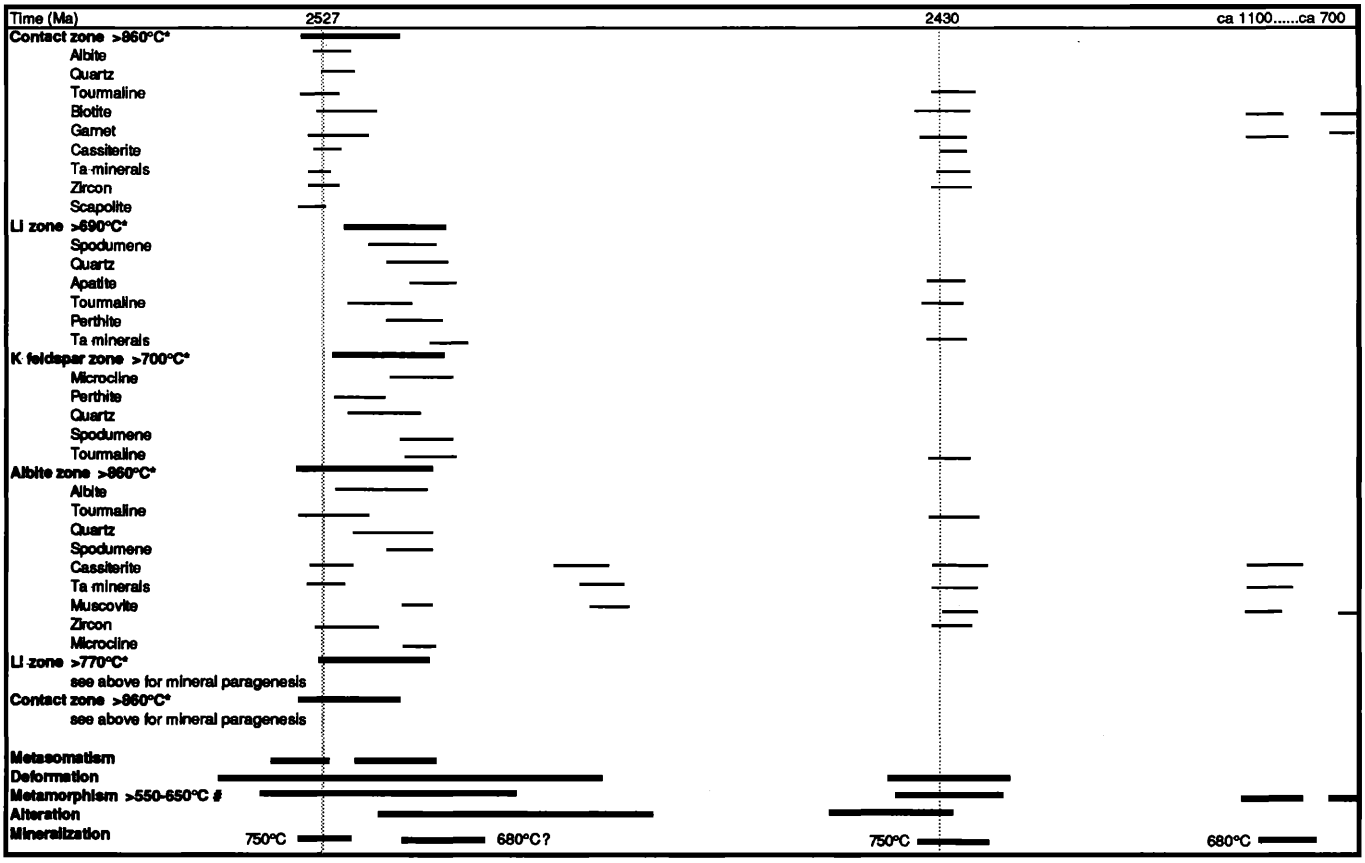


FIG. 5. Summary of the paragenetic sequence and timing of crystallization of the main minerals in each zone of the Greenbushes pegmatite compared to the temperature data of Han (1991) and the timing of deformation and metamorphic events.

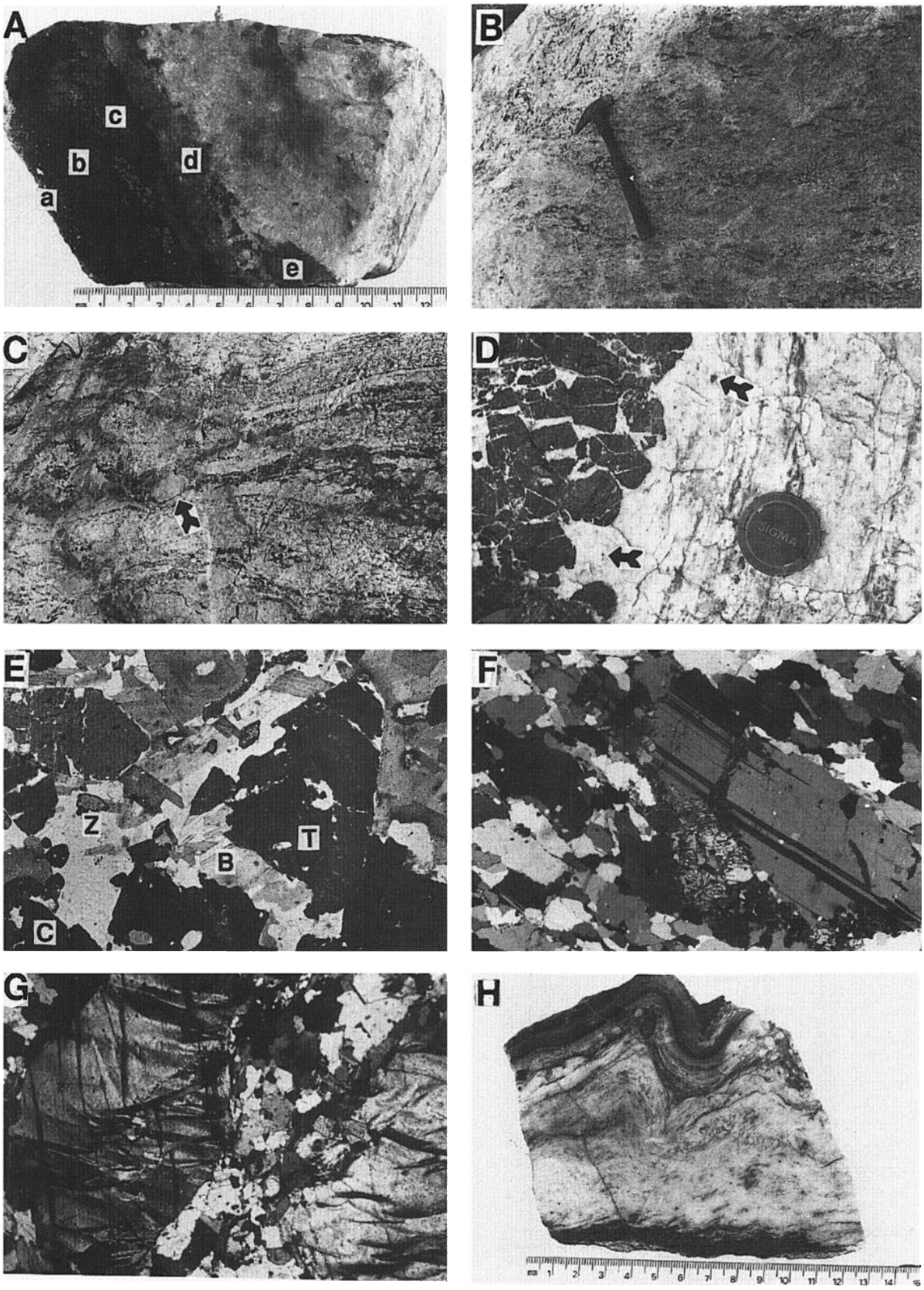
A
a
b
c
d
e
B
C
D
SIGMA
E
Z
T
B
C
F
G
H

(Figs. 5 and 6A). Many of the mafic-ultramafic host rocks are carbonated, and these contain euhedral crystals of Ca scapolite and epidote often in association with calcite. Layers around the xenoliths in the pegmatite consist of garnet, scapolite, biotite, arsenopyrite, tourmaline, cassiterite, zircon, uraninite, tantalite, and albite (Fig. 6A and E). The cementing of fractured and pulled-apart tourmalines by spodumene, biotite, and garnet, the association of biotite and garnet with tourmaline, tantalite, uraninite, and cassiterite, and also the growth of biotite and garnet across many pegmatite contacts, suggest that deformation, early crystallization of the pegmatite, including crystallization of tin and tantalum minerals and zircon, and metamorphism were all essentially synchronous.

The hanging-wall lithium zone in the main pegmatite is generally richer (up to 5% $Li_2O$, equivalent to 60–80% spodumene) than the footwall lithium zone, which is laterally more continuous (Fig. 3). Lithium zones are also developed in the centers of subsidiary albititic pegmatite dikes and pods to the north of the main pegmatite (Fig. 3). The lithium zones in the main pegmatite generally contain coarse-grained euhedral spodumene intergrown with quartz, which forms white and pink lustrous units at the top of both the hanging-wall and footwall zones (Fig. 6B). The spodumene crystals are finer grained at the center of the lithium zones, occurring as granular intergrowths with quartz and K feldspar. Intercalations of quartz-albite or monomineralic lenses of blocky perthitic microcline also occur in this part of the lithium zone. Accessory minerals in the lithium zone of the pegmatite include apatite, tourmaline, muscovite, beryl, and tantalite (Fig. 5).

Textural relationships suggest that tourmaline formed early in the paragenetic sequence with later contemporaneous growth of quartz and spodumene (Fig. 5), which according to Han (1991) crystallized at 770°C in the footwall lithium zone and 690°C at 5 kbars in the hanging-wall lithium zone. There are no textures indicative of petalite replacement by spodumene, such as the fibrous quartz-spodumene intergrowths that are pseudomorphs of petalite laths. Therefore, the sequence is interpreted as being consistent with crystallization of a lithium- and silica-rich magma in the system albite-quartz-eucryptite-$H_2O$. The formation of essentially feldspar-free spodumene-quartz assemblages, however, requires high temperatures. In this case, unless crystallization pressures are very high, petalite is the stable lithium mineral and this later reverts to spodumene. The absence of petalite and the presence of iron-poor spodumenes suggest that the pressure of formation of the Greenbushes Pegmatite Group was in the region of 5.5 kbars (Partington, 1988, 1990a), where spodumene is stable at much higher temperatures (e.g., London and Burt, 1982). This is confirmed by the fluid inclusion studies of Han (1991).

The K feldspar zone occurs at, or near, the hanging-wall contact of the main pegmatite and reaches a maximum thickness of over 75 m in the center of the main pegmatite (Figs. 3 and 4). K feldspar zones are rare outside the main pegmatite, and where they do occur as discrete pods and smaller dikes, they are commonly concentrated in the hanging-wall portions of subsidiary pegmatites. No significant mineralization has been discovered in any of the K feldspar zones and the only ore minerals associated with K feldspar are minor amounts of tantalite and spodumene. This zone in the main pegmatite consists largely of pods of perthitic microcline and coarse-grained quartz, which are locally intergrown with muscovite (Fig. 6C). Fluid inclusion work suggests that the perthitic microcline crystallized at 700°C at 5 kbars (Han, 1991). In many cases there is a primary layering defined by fine-grained tourmaline and albite bands alternating with quartz-microcline bands (Fig. 6C). This banding is not continuous and is overprinted by $D_2$ fabrics. Megacrysts of coarse-grained K feldspar with irregular outlines occur within, and are wrapped by, the layering; conversely, other crystals truncate the layering. Accessory minerals include coarse-grained tourmaline, spodumene, beryl, and apatite. Textural relations in the K feldspar zone, such as graphic intergrowths between quartz and K feldspar, indicate that quartz and microcline crystallized together and that they were followed by spodumene and tourmaline (Fig. 5).

The albite zone can be described in terms of two main assemblages: albite-quartz, and quartz-albite ± microcline ± muscovite (Bettenay et al., 1985). The albite zone occupies the lower footwall region of the main pegmatite, although farther south this zone occupies a more central position within the sequence (Figs. 3 and 4). Albite pegmatites also commonly occur as dikes and pods to the north of the main pegmatite (Figs. 3 and 4). Many of the albite pegmatites

FIG. 6. Photographs and photomicrographs of the Greenbushes pegmatite. A. Typical border zone in the pegmatite from the 1160 level of the underground mine (12,900 m N 9,800 m E). The reaction assemblages from the contact into the pegmatite are (a) biotite-arsenopyrite, (b) tourmaline-biotite-zircon-epidote, (c) tourmaline-cassiterite-biotite, (d) tourmaline-garnet-cassiterite-zircon-uraninite, and (e) albite-cassiterite-uraninite. B. Lithium zone from the Lemonade Springs area (Fig. 3), showing a well-defined primary fabric. C. Primary layering in the K feldspar zone of the Greenbushes pegmatite from the Highway shoot area (Fig. 3), which is overprinted by $D_3$ shear fabrics. Note the wrapping of the primary layering around a K feldspar megacryst (arrow). D. Albite zone, from the 1160 level of the underground mine (12,900 m N 9,800 m E), with primary layering defined by albite and quartz layers. Note the concentration of ore minerals (arrow) at the contact between the albite zone and a tourmaline subzone. E. Photomicrograph of an ore zone in a tourmaline subzone of the albite zone from the 1160 level of the underground mine (12,900 m N 9,800 m E). Note the association of zircon (grain directly above Z) with cassiterite (C) and zoned tourmalines (T), and the pulled-apart crystal (T) of tourmaline cemented by biotite (B). Plane-polarized light, field of view approx 3.5 mm wide. F. Photomicrograph of a deformed and pulled-apart albite crystal, cemented by spodumene and microcline, set in a flattened recrystallized matrix of quartz crystals, from the 1160 level of the underground mine (12,900 m N 9,800 m E). Note shear fabric defined by flattened crystals and kinked albite twin planes. Crossed polars, field of view approx 14 mm wide. G. Kink bands in a large primary muscovite crystal from the 1160 level of the underground mine (12,900 m N 9,800 m E). Plane-polarized light, field of view approx 3.5 mm wide. H. Photograph of a microscopic asymmetric fold in a greissen zone from the 1160 level of the underground mine (12,900 m N 9,800 m E); the form surface of the fold is a fabric defined by fine-grained albite, muscovite, garnet, beryl, and apatite.

TABLE 1. Average Gneiss and Granotoids in the Pegmatite District and Various Macroscopic Zones from the Greenbushes Pegmatite

| | 1 | 2 | 3 | 4 | 5 | 6 | 7 | 8 | 9 | 10 |
|---|---|---|---|---|---|---|---|---|---|---|
| Major Elements (wt %) | | | | | | | | | | |
| $SiO_2$ | 69.14 | 66.64 | 70.14 | 68.75 | 74.57 | 68.48 | 73.74 | 73.75 | 75.68 | 76.90 |
| $TiO_2$ | 0.06 | 0.07 | 0.06 | 0.07 | 0.04 | 0.06 | 0.19 | 0.11 | 0.04 | |
| $Al_2O_3$ | 14.67 | 15.66 | 14.28 | 13.93 | 13.20 | 15.06 | 13.94 | 13.91 | 13.2 | 13.40 |
| FeO[1] | 1.31 | 1.74 | 1.14 | 0.73 | 0.84 | 1.60 | 0.85 | 2.00 | 1.64 | 1.20 |
| MgO | 0.23 | 0.27 | 0.22 | 0.28 | 0.40 | 0.23 | 0.16 | 0.40 | 0.13 | 0.20 |
| CaO | 0.97 | 1.40 | 0.79 | 0.31 | 0.39 | 1.28 | 0.45 | 1.73 | 1.17 | 1.26 |
| $Na_2O$ | 4.82 | 6.53 | 4.14 | 2.27 | 1.33 | 6.10 | 2.57 | 3.72 | 3.86 | 3.92 |
| $K_2O$ | 2.07 | 0.66 | 2.64 | 5.75 | 4.78 | 0.89 | 1.50 | 3.92 | 4.05 | 3.00 |
| $P_2O_5$ | 0.61 | 0.96 | 0.47 | 0.22 | 0.22 | 0.82 | 0.20 | 0.03 | 0.05 | 0.04 |
| Trace Elements (ppm) | | | | | | | | | | |
| Li | 2,325 | 955 | 2,873 | 907 | 1,460 | 1,008 | 12,734 | 12 | 10 | 10 |
| Cs | 501 | 219 | 613 | 1,119 | 612 | 308 | 374 | | | |
| Rb | 4,159 | 1,160 | 5,358 | 11,999 | 9,114 | 1,693 | 2,656 | 134 | 129 | 104 |
| Sr | 65 | 55 | 69 | 131 | 95 | 47 | 34 | 251 | 84 | 130 |
| $Ta_2O_5$ | 183 | 246 | 158 | 88 | 93 | 233 | 86 | | | |
| $Nb_2O_5$ | 132 | 192 | 107 | 33 | 55 | 178 | 61 | | | |
| Sn | 707 | 1,363 | 444 | 12 | 224 | 1,000 | 179 | 1.68 | 1.5 | 2.0 |
| Be | 125 | 129 | 123 | 31 | 126 | 146 | 74 | | | |
| Zr | 27 | 42 | 20 | 8 | 6 | 36 | 11.5 | | | |
| Ni | 2–25 | 14 | 11 | 12 | 10 | 12 | 12 | | | |
| As | 79 | 141 | 45 | 31 | 4 | 104 | 60 | | | |
| U | 12.6 | 21.4 | 10.0 | 6.6 | 4.7 | 16.3 | 6.2 | | | |
| Th | 11.3 | 25.3 | 7.2 | 2.3 | 3.3 | 16.5 | 3.1 | 34.7 | 24.0 | 27.0 |
| Ratios (by weight) | | | | | | | | | | |
| K/Rb | 0.02–20 | 6.5 | 4.95 | 3.92 | 4.25 | 5.93 | 5.23 | 356 | 305 | 267 |
| K/Li | 0.02–438 | 16.84 | 36.91 | 93.57 | 29.28 | 14.05 | 4.84 | 3,520 | 7,582 | 4,339 |
| Nb/Ta | 0.12–1.66 | 0.80 | 0.65 | 0.40 | 0.55 | 0.79 | 0.71 | | | |
| Sr/Rb | 0.006–1.68 | 0.20 | 0.04 | 0.01 | 0.01 | 0.12 | 0.03 | 4.77 | 0.76 | 2.02 |

Data for 8, 9, and 10 adapted from Blockley (1980); all other data from Bettenay et al. (1985) and Partington (1988)

Samples: 1, Greenbushes pegmatite; 2, northern pegmatites; 3, main pegmatite; 4, K feldspar zone; 5, greisenized pegmatite; 6, albite zone; 7, lithium zone; 8, biotite granite; 9, gneiss; 10, orthogneiss

[1] Total Fe as FeO

contain significant amounts of cassiterite and tantalite (Fig. 6D and E). Aligned aggregates of fractured and fragmented, euhedral-anhedral albite crystals of up to 3 cm in length commonly occur in the albite pegmatites. In some areas the alignment of plagioclase crystals and twin planes appears to be a primary feature, as suggested by the presence of internal crystal zoning, lack of deformational textures, and euhedral form of the plagioclase crystals. The larger albite crystals behaved in a brittle fashion, and consequently many crystals with well-developed albite twin laws are so deformed that the present crystal forms bear no relationship to the original crystal shape (Fig. 6F). These crystals commonly contain inclusions of mica, tantalite, and cassiterite, are also embayed by K feldspar and spodumene, contain fractures infilled by K feldspar, and form pulled-apart fragments cemented by K feldspar. Tourmaline is the first mineral to crystallize in the paragenetic sequence and this formed at 860°C and 5.5 kbars (Fig. 5; Han, 1991). Crystallization of tourmaline continued with the coeval crystallization of albite, tantalite, and cassiterite ± zircon, whereas spodumene, apatite, beryl, and K feldspar formed late in the crystallization sequence (Fig. 5).

The macroscopic zonal sequence has many smaller subzone variations, e.g., muscovite-apatite-beryl in the K feldspar zone, tourmaline-rich layers in the albite zone (described above), and quartz layers in the lithium zone. These variations are minor, are not continuous in three dimensions, and are therefore not considered to be separate zones (Paterson, 1983; Bettenay et al., 1985, 1988; Partington, 1986, 1988).

Tourmaline-rich units generally occur as subzones within the albite zone (Paterson, 1983). The tourmaline-rich zones generally occur in the immediate contact zone of the pegmatite associated with amphibolites, around mafic xenoliths, and toward the footwall of the albite zone in the main pegmatite. Smaller tourmaline-rich zones (up to 4 m thick) are also present in the northern pegmatites, which are characterized by very coarse grained tourmaline crystals and high abundances of apatite, beryl, and cassiterite with interstitial albite, quartz, and muscovite (Fig. 6D). Primary igneous textures are present in some of the less deformed areas of the tourmaline zones forming tourmaline "rosettes" or "suns," which resemble comb and orbicular structures in granitoids (Fig. 2D). Minerals oriented perpendicular to pegmatite host-rock contacts, and on a smaller scale on xenoliths of country rock, are also common (Fig. 2C and E).

Tourmaline and albite crystals are commonly aligned, forming an imbricate fabric defined by the long axes of tourmaline grains and albite twin planes (Fig. 6D). This imbrication is associated with a layering in the pegmatite, which is similar to flow structures in granitoids and the "line rock" described by Page et al. (1953) in pegmatites from the Black Hills, South Dakota. Most tourmalines belong to the schorl-elbaite series and occur as euhedral crystals up to 30 cm in

length. Generally tourmalines that are longer than 5 mm are color zoned in cross section (Fig. 6E), having a pleochroic light to dark blue core and an outer rim that varies from yellow to light khaki to dark brown-green. The tourmalines are generally not recrystallized and are deformed by brittle fracture (Fig. 6D), although some crystals contain subgrains.

Numerous small, 1- to 4-m-wide greisenlike zones containing muscovite, beryl, garnet, tourmaline, spodumene, monazite, microlite, and albite also occur (Fig. 6H). These assemblages are always associated with shear zones that postdate pegmatite intrusion. The greisen zones are folded and crenulated and the muscovite is aligned in a fabric, which is axial planar to the complexly folded and transposed quartz veins. The garnets and small euhedral tourmalines enclose an earlier foliation and are also wrapped by a later foliation, suggesting that the alteration was synchronous with shearing.

Major element geochemistry of the Greenbushes Pegmatite Group is essentially similar to that reported for granitoids and pegmatites (Table 1). Trace element values, with the exception of Ti, are similar to values reported from other rare element pegmatites (Table 1). High Ti values occur in certain zones in the pegmatite and are commonly associated with mafic xenoliths and tourmaline-rich subzones. Fractionation indices, using whole-rock and mineral data (Paterson, 1983), are similar to those reported by Černý (1982a) for other rare element pegmatites (Table 1). These values indicate that extreme fractionation occurred beyond the levels observed in other igneous and postmagmatic assemblages. Fractionation indices such as K/Rb, K/Li, Sr/Rb, Nb/Ta, and FeO/FeO + MgO in tourmaline vary continuously across the pegmatite (Fig. 7). These trends also indicate, as does the zonal scheme, that the more fractionated values come from the outer zones of the main pegmatite (Figs. 3, 4, and 7).

The macroscopic zonation in the Greenbushes pegmatite is unusual, and perhaps unique, in that those zones normally expected to crystallize last and hence in the center of the pegmatite (e.g., lithium zones; Norton, 1983) occur as footwall and hanging-wall zones (Figs. 3 and 4). Structural studies (Partington, 1988, 1990a and b) suggest that the pegmatite was intruded and crystallized during $D_2$ deformation and the reverse zoning may have formed in a manner similar to antitaxial veins (e.g., Ramsay and Huber, 1983), where addition of newly crystallized material occurred along the vein wall contact as deformation proceeded (cf. curved tourmaline crystals shown in Fig. 2E and curved fibers found in antitaxial veins). Movements along the Donnybrook-Bridgetown shear zone (Partington, 1988, 1990a and b) controlled not only the intrusion of the pegmatite but also its eventual crystallization and internal zoning.

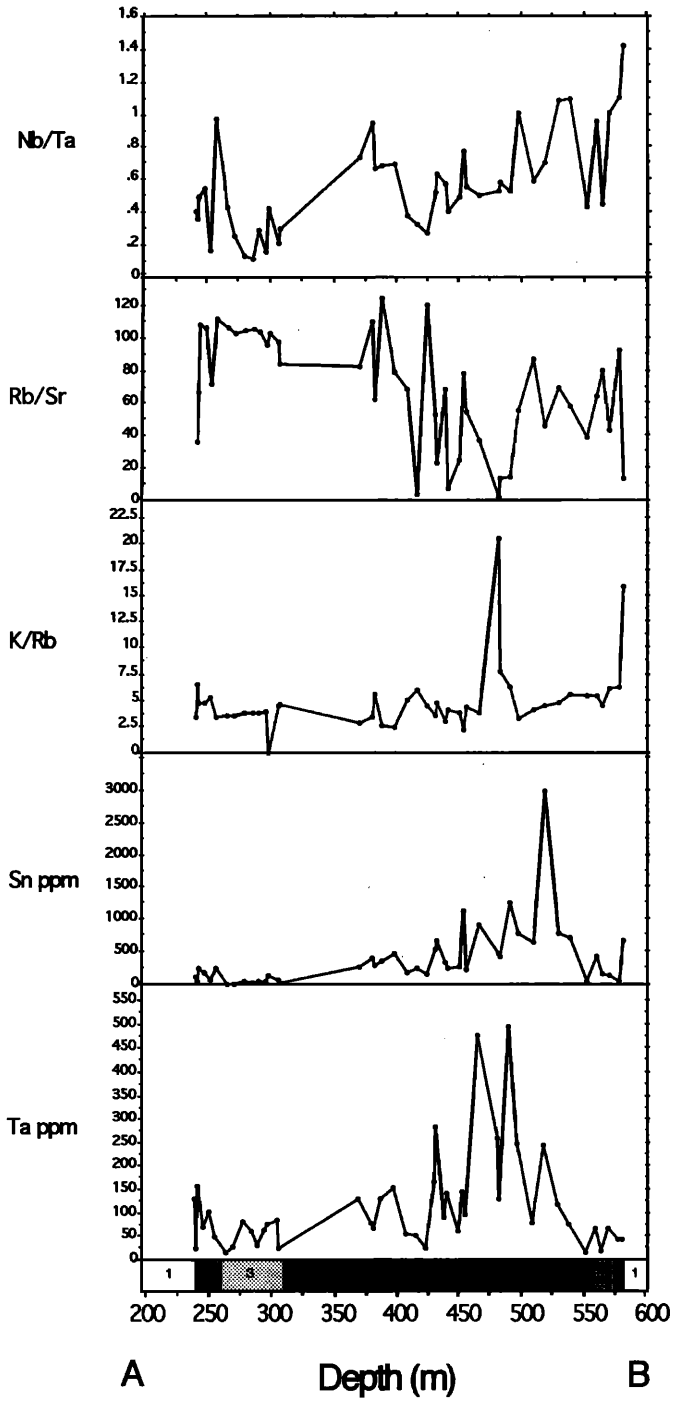


FIG. 7. Fractionation indices across the pegmatite compared to the macroscopic zoning and Sn and Ta grades. See Figure 3 for location of the section A-B through the pegmatite. (1) amphibolite, (2) Li zone, (3) K zone, (4) Na zone.

*Mineralization*

Ore mineralogical studies identified more than ten Ta-bearing phases (Bettenay et al., 1985), including Ta ilmenite and Ta rutile (strüverite). Cassiterite is the main Sn-bearing phase, which occurs as euhedral swallow-tailed crystals. When cassiterite is deformed it also forms pull-apart and cataclastic textures similar to the early crystallized tourmaline (Fig. 8A and B). Early formed tantalum minerals, mainly wodginite and ixiolite, occur as inclusions within cassiterite and tourmaline crystals. In contrast to the early tantalum minerals, the later coexisting tantalum phases (tantalites and tapiolites) in silicates are Sn free and generally occur in fractures and pull-aparts in the early silicate phases (Fig. 8C, D, and G). Characteristic ore zone accessories associated with the early crystallized mineralization include zircon, monazite, uraninite, and probable euxenite (Fig. 6E; Bettenay et al., 1985).

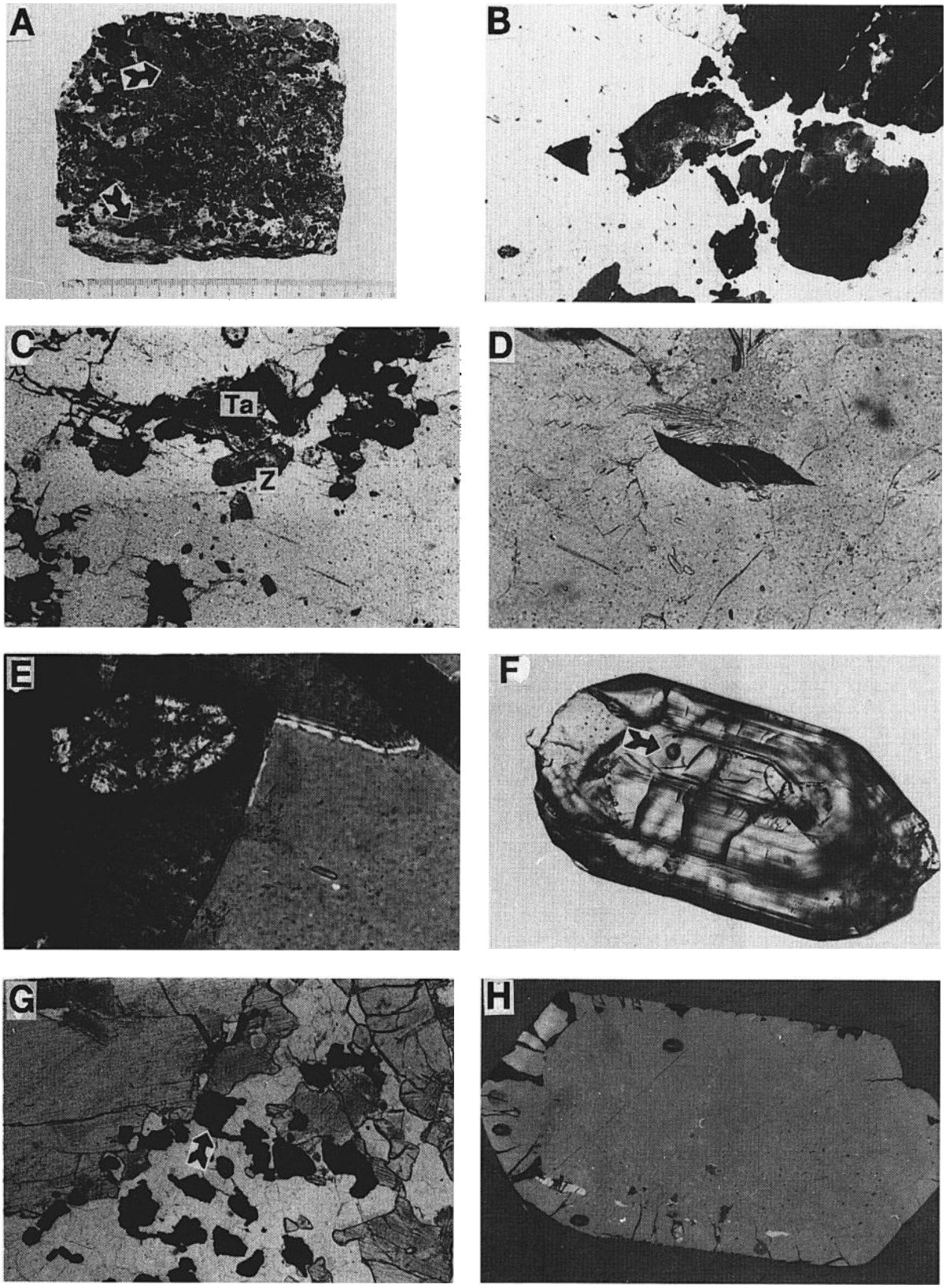
A
B
C
Ta
Z
D
E
F
G
H

Micron-scale inclusions of a distinctive Ta-rich cassiterite characterize some of the spodumene-quartz zones. Microlite is an important and widespread Ta phase in these zones and contains low U, Ce, and Th, with variable Ti (Bettenay et al., 1985). This tantalum mineralization tends to be late and is associated with zircon, monazite, pollucite, and lepidolite (Fig. 8C).

Paragenetic and fluid inclusion studies suggest that three phases of Sn and/or Ta mineralization occurred (Han, 1991; Partington, 1988, 1990b). The first is related to initial crystallization of tourmaline at a temperature of 750°C at 5 kbars (Figs. 6E and 8A). The second phase of mineralization appears to have occurred during deformation and metamorphism, but still during crystallization of the pegmatite at a temperature of 680°C at 5 kbars (Fig. 8C and G). The third phase is associated with the greisen and metasomatic zones in the pegmatite and appears to be related to a hydrothermal event, which occurred at 620°C at 5 kbars (Fig. 6H). Preserved low-strain textures in the early crystallized mineralized zones are typically those of magmatic crystallization (Figs. 6E and 8A), in which ore minerals crystallized at an early stage, in association with tourmaline, with other enriched accessories (notably zircon and uraninite). The second and third phases of mineralization were the result of hydrothermal processes at the end of, or after, magmatic crystallization of the pegmatite, and these upgraded the preexisting early mineralization, which is more typically associated with microlite rather than tantalite (Fig. 8C and G). Both stages of mineralization are associated with zircon growth, potentially allowing isotopic age dating of the two mineralizing events to be made.

## Geochronology

### *Methodology*

Fresh whole-rock samples were collected from the Cowan Brook Dam granitoid from a locality approximately 1 km to the northwest of the Greenbushes pegmatite (Fig. 1B). Whole-rock samples were crushed in a precleaned jaw crusher and ground in an agate swing mill to minimize Pb contamination. Lead was extracted at the University of Western Australia and mass analyzed at Curtin University of Technology utilizing a VG354 multicollector mass spectrometer and established methods (McNaughton and Bickle, 1987). Isotopic analyses were referenced to NBS-981, and analytical uncertainty of all Pb isotope ratios is ±0.15 percent ($2\sigma$).

Descriptions of the samples and zircons are given in Table 2 and the location of areas shown in Figures 1A, B, and 3. Zircon is an abundant accessory in the younger granitoids, is a major accessory mineral in most of the major zones of the pegmatite, and is especially associated with mineralization. Fresh-rock samples (about 2 kg) were selectively collected from a granitoid at the Millstream dam (Fig. 1B) and underground exposures of the Greenbushes pegmatite (Table 2). These samples were collected and broken down in the field with a hammer. A representative hand specimen was chosen for thin sections and the remaining material was washed in water, dried, and crushed in a precleaned jaw crusher. Samples for zircon extraction were lightly crushed in a tungsten carbide tema mill until they passed through a 60# nylon sieve.

A bulk sample from the heavy mineral concentrate from the Greenbushes mill was also collected for zircon analysis. This sample was collected from a batch of ore mined from the albite zone of the pegmatite in the Cornwall Hill area (Fig. 3). To minimize possible contamination, the bulk sample was collected after the mill had been cleaned and half way through processing the batch of ore from the pegmatite. The ore zone from which the sample was collected is near the center of the pegmatite and no host-rock inclusions were observed during mining. Since the zircons analyzed from the bulk sample have evidence of radiation damage, contain inclusions of cassiterite, and have distinctively low Th/U and $^{208}Pb/^{206}Pb$ (Fig. 9; discussed below), similar to those sampled from the underground mine, they are taken to be from the pegmatite. The bulk sample and crushed rock samples were passed over a Wilfley table to concentrate the heavy fraction, which was then dried and passed through an electromagnetic separator and then bromoform to concentrate the heavy nonmagnetic grains including zircon. Zircon was further concentrated using diiodomethane and then handpicked under ethanol with the aid of a binocular microscope to produce the final concentrate.

The zircons from the granitoids are euhedral with good growth zoning and evidence for overgrown cores (Fig. 8F). Two zircon types have been identified in the pegmatite. The first is associated with the ore minerals such as cassiterite, tantalite, and uraninite and formed early in the crystallization sequence (Figs. 6E and 8H). These crystals tend to be euhedral to subhedral, up to 3.5 mm in size, and often display internal zoning with evidence of resorption and radial cracks thought to relate to alteration affecting areas of radiation

FIG. 8. Photographs and photomicrographs of the Greenbushes pegmatite. A. Typical high-grade ore from the 1160 level of the underground mine (12,900 m N 9,800 m E). Note pulled-apart cassiterites and tourmalines (arrows). B. Photomicrograph of high-grade ore from the 1160 level of the underground mine (12,900 m N 9,800 m E), showing cassiterite and Ta minerals in cassiterite and tourmaline. Plane-polarized light, field of view approx 1.4 mm wide. C. Zircon (Z) associated with tantalum-bearing phases (Ta) in fractured albite from the 1160 level of the underground mine (12,900 m N 9,800 m E). Plane-polarized light, field of view approx 14 mm wide. D. A pulled-apart tantalite crystal, from the 1160 level of the underground mine (12,900 m N 9,800 m E), which is associated with the second phase of mineralization. Plane-polarized light, field of view approx 1.4 mm wide. E. Example of zoned zircon from the Millstream Dam granitoid. Plane-polarized light, field of view approx 1.4 mm wide. F. Photomicrograph of an analyzed zircon grain from the Millstream Dam granitoid. Note the zoning, central core to the zircon, and microprobe burn mark on the top left of the central core. Plane-polarized light, field of view approx 3.5 mm wide. G. An example of tantalum mineralization (arrow) associated with spodumene within the lithium zone of the pegmatite from the Lemonade Springs area (Fig. 3). Plane-polarized light, field of view approx 14 mm wide. H. An example of an analyzed zircon from the Greenbushes pegmatite. Note oval burn marks and radial cracks in rim zones. Reflected light, field of view approx 3.5 mm wide.

TABLE 2. Location and Sample Descriptions of the Geochronological Samples from the Granitoids and Greenbushes Pegmatite

| Field no. | University of Western Australia no. | East-north RL | Rock type | Brief rock-zicron description |
|---|---|---|---|---|
| Cowan Brook Dam granitoid (Fig. 1) | | | | |
| | 104056 to 104070; see Table 3 | 400,000E AMG, 253,500N AMG, surface sample | Leucogranite | Metamorphosed granitoid with accessory garnet and tourmaline |
| Millstream Dam granitoid (Fig. 1) | | | | |
| LOC39 | 104054 | 401,000E AMG, 253,500N AMG, surface sample | Sheared biotite orthogneiss | |
| Zircon 19 | | | | Euhedral massive to weakly zoned core |
| Zircon 23 | | | | Fragment of zircon; no internal zoning |
| Zircon 28 | | | | Euhedral zircon with continuous, concordant, euhedral internal zoning |
| Zircon 30 | | | | Euhedral zicron with rim of euhedral zoning about a more massive core |
| Zircon 34 | | | | As zircon 28 |
| Greenbushes pegmatitie: Mine 1,160 level (Fig. 3) | | | | |
| GC-1 | 104047 | 9503 mine grid, 12892 mine grid, 1160 mine RL | Undeformed Na pegmatite | |
| Zircon 2 | | | | Euhedral zircon with external radiation damage; inclusions of uraninite and cassiterite |
| Zircon 5 | | | | Subhedral zircon with evidence of radiation damage |
| Greenbushes pegmatite: Mine 1160 level (Fig. 3) | | | | |
| GC-3 | 104088 | 9472 mine grid, 12971 mine grid, 1160 mine RL | Undeformed Na pegmatite | |
| Zircon 1 | | | | Anhedral zircon with no overgrowths or internal zoning |
| Zircon 2 | | | | Fragment; undamaged with no inclusions |
| Zircon 8 | | | | Fragment with possible overgrowth |
| Zircon 9 | | | | Fragment; undamaged with no inclusions |
| Zircon 11 | | | | Anhedral zircon with radiation damage and inclusions |
| Zircon 15 | | | | Euhedral zircon with radiation damage and weakly zoned |
| Greenbushes pegmatite: Mine open-cut bulk sample (Fig. 3) | | | | |
| GC-35 | 104055 | 9700 mine grid, 12620 mine grid, 1300 mine RL | Cornwall Hill mineralized pegmatite | |
| Zircon 1 | | | | Euhedral zircon with radiation damage and inclusions |
| Zircon 2 | | | | Euhedral zircon with little radiation damage and few inclusions |
| Zircon 4 | | | | As zircon 2 |
| Zircon 5 | | | | As zircon 1 |
| Zircon 6 | | | | Euhedral zircon |

Abbreviations: AMG = Australian map grid, RL = relative level

damage (Fig. 8H). The second type of zircon formed late as smaller grains associated with microlite at grain boundaries and within fractures in albite and tourmaline grains (Fig. 8C). Many of the zircons in the pegmatite contain minor inclusions of tantalum and cassiterite, indicating that zircons formed during crystallization of the pegmatite.

Zircon populations from each sample were mounted and analyzed with the SHRIMP ion microprobe according to methods described in Compston et al. (1984) and Williams et al. (1984). The common Pb correction of zircon analyses utilized the composition of coeval Pb (Cumming and Richards, 1975; model III) to remove all $^{204}Pb$. Zircon standard SL3 was used as the calibrating standard with an assigned age of 555 Ma. Common Pb isotope analyses follow methods described by McNaughton and Bickle (1987). All calculations involving lead isotope data use the decay constants determined by Jaffey et al. (1971): $\lambda^{238}U = 0.155125 \times 10^{-9}\ yr^{-1}$ and $\lambda^{235}U = 0.98485 \times 10^{-9}\ yr^{-1}$; isotopic parameters follow Tatsumoto et al. (1973). Regressions of zircon data and calculation of uncertainties are described by Ludwig (1980), whereas common Pb isotope data are regressed by the method of York (1969).

TABLE 3. Cowan Brook Dam Pb Isotope Compositions of Whole Rocks

| Sample no. | $^{206}Pb/^{204}Pb$ | $^{207}Pb/^{204}Pb$ | $^{208}Pb/^{204}Pb$ |
|---|---|---|---|
| 104056 | 20.853 | 16.082 | 35.677 |
| 104057 | 19.358 | 15.814 | 35.331 |
| 104058 | 21.170 | 16.112 | 35.284 |
| 104062A | 20.687 | 16.064 | 35.284 |
| 104062B | 20.665 | 16.050 | 35.420 |
| 104063 | 19.977 | 15.935 | 35.403 |
| 104064 | 18.678 | 15.694 | 37.884 |
| 104065 | 20.049 | 15.926 | 36.952 |
| 104066 | 19.558 | 15.858 | 35.773 |
| 104067 | 21.066 | 16.093 | 35.305 |
| 104068 | 20.335 | 15.964 | 35.068 |
| 104069 | 20.750 | 16.056 | 35.187 |
| 104070 | 18.987 | 15.747 | 35.307 |

Error in ratios is ±0.15% (2$\sigma$)

## Results

### *Age of the Cowan Brook Dam granitoid*

Whole-rock Pb isotope analyses were carried out on the Cowan Brook Dam granitoid samples (Table 3). These fall on a single isochron, which defined an age of 2588 ± 93 Ma (2$\sigma$) with a two-stage model source $\mu_1$ value of 8.08 ± 0.05 and a mean square weighted deviation (MSWD) value of 1.6 (Fig. 9). The large uncertainty in the age reflects the low spread of the data along the isochron and hence the need for the more precise U-Pb zircon geochronology of this, or structurally coeval, suites. The model $\mu_1$ value (source $^{238}U/^{204}Pb$) is slightly above the normal mantle range of 7.5 to 8.0 (Moorbath and Taylor, 1981), which is compatible with an older source terrane such as 3.1 Ga gneisses of the district (Fletcher et al., 1983).

### *Age of the Millstream Dam granitoid*

Results of the zircon U-Pb studies on the Millstream Dam granitoid are shown in Figure 10 and presented in Table 4. All the zircon rims yield a common $^{207}Pb/^{206}Pb$ ratio corresponding to a pooled age of 2577 ± 4 Ma (2$\sigma$). This is within error of the imprecise Pb-Pb whole-rock age for the Cowan Brook Dam granitoid. One zircon grain has a core of indistinguishable age to the rims, whereas two grains (19 and 30) have slightly older cores (Fig. 10 and Table 4) giving pooled ages of 2605 ± 9 and 2610 ± 10 Ma, respectively. These zircon cores may be partly annealed xenocrysts from an older terrane, or early formed zircons that crystallized during the initial stages of granitoid magmatism. There is no unequivocal evidence from this pluton to indicate which of these alternatives is correct. However, since there is evidence of granitoid intrusion at 2612 ± 5 Ma elsewhere in the Balingup metamorphic belt associated with $D_2$ deformation (e.g., the Logue Brook granitoid; Fig. 1B; Compston et al., 1986), it is interpreted that the older zircon cores in the Millstream Dam granitoid are probably xenocrystic. It follows that the Millstream Dam granitoid may be composed of at least two intrusive events, with the enclosed orthogneiss an older phase, intruded at about the same time as the Logue Brook granitoid.

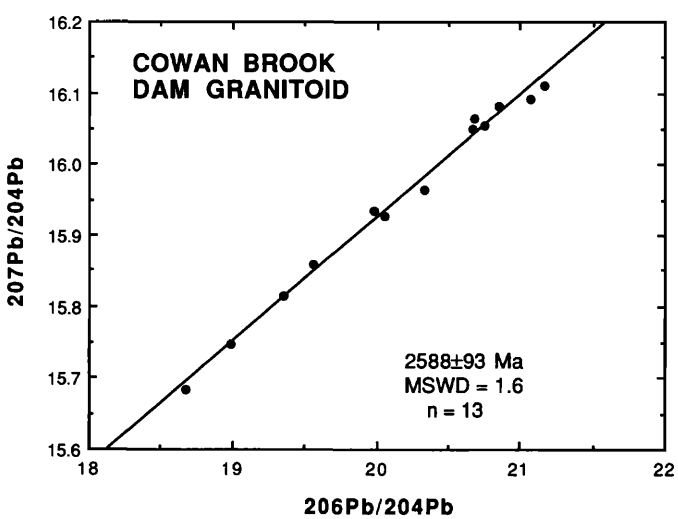


FIG. 9. Common lead isochron diagram for whole rocks from the Cowan Brook Dam granitoid.

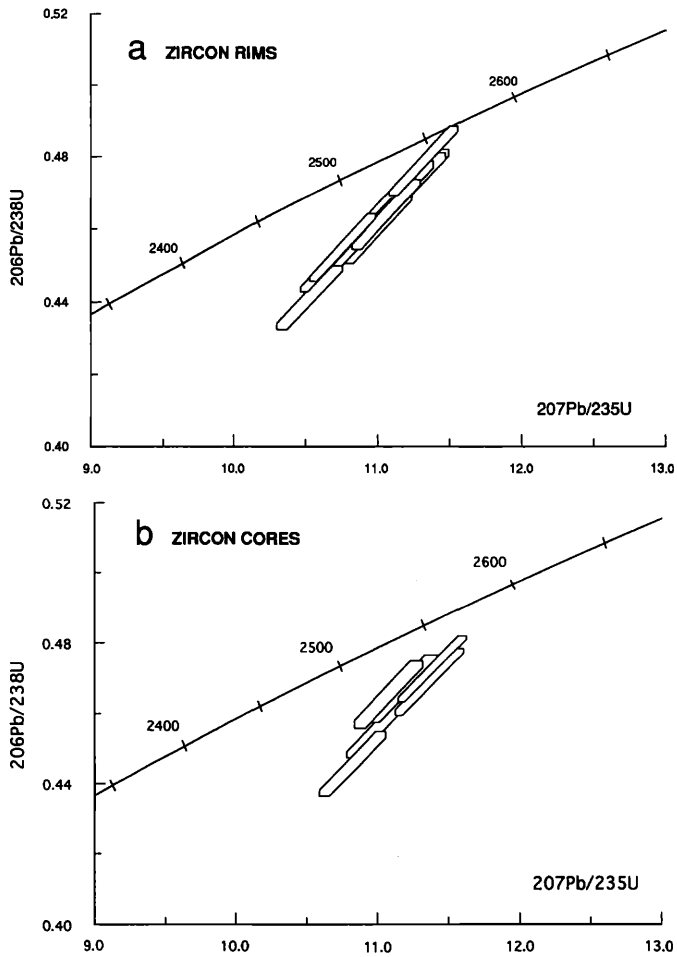


FIG. 10. Concordia plot of zircon data from the Millstream Dam granotoid. a. Zircon rims have indistinguishable $^{207}Pb/^{206}Pb$ corresponding to a pooled age of 2577 ± 4 Ma. b. Zircon core analyses. Error boxes shown are 1$\sigma$.

### *Age of the Greenbushes pegmatite*

The zircon results from the three pegmatite samples analyzed using the SHRIMP ion microprobe are given in Table

TABLE 4. Zircon Isotope Results from the Millstream Dam Granitoid Sample (UWA-104054)

| Grain spot | f%[1] | $^{204}$Pb (ppb) | U (ppm) | Th (ppm) | $^{208}$Pb/$^{206}$Pb | $^{206}$Pb/$^{238}$U | $^{207}$Pb/$^{235}$U | $^{207}$Pb/$^{206}$Pb ($\pm 2\sigma$) | Minimum age (Ma $\pm 2\sigma$) |
|---|---|---|---|---|---|---|---|---|---|
| 19-1 rim | 0.30 | 60 | 674 | 79 | 0.0353 | 0.473 | 11.24 | 0.1724 ± 19 | 2582 ± 21 |
| | 0.12 | 24 | 682 | 80 | 0.0345 | 0.460 | 10.99 | 0.1731 ± 19 | 2588 ± 21 |
| 19-2 core | 0.14 | 56 | 1,359 | 161 | 0.0353 | 0.469 | 11.36 | 0.1755 ± 13 | 2661 ± 15 |
| | 0.04 | 16 | 1,374 | 160 | 0.0339 | 0.473 | 11.38 | 0.1745 ± 13 | 2602 ± 13 |
| 23-1 rim | 0.34 | 73 | 732 | 83 | 0.0331 | 0.472 | 11.22 | 0.1725 ± 18 | 2582 ± 18 |
| | 0.11 | 23 | 742 | 83 | 0.0329 | 0.459 | 10.91 | 0.1723 ± 16 | 2580 ± 16 |
| 23-2 rim | 0.45 | 80 | 628 | 117 | 0.0520 | 0.456 | 10.78 | 0.1716 ± 21 | 2573 ± 20 |
| | 0.10 | 17 | 630 | 118 | 0.0566 | 0.442 | 10.52 | 0.1727 ± 18 | 2583 ± 17 |
| 28-1 rim | 0.32 | 97 | 1,048 | 146 | 0.0351 | 0.466 | 11.02 | 0.1714 ± 16 | 2571 ± 15 |
| | 0.08 | 25 | 1,064 | 145 | 0.0355 | 0.479 | 11.31 | 0.1713 ± 14 | 2570 ± 13 |
| 30-1 core | 0.40 | 69 | 605 | 95 | 0.0450 | 0.457 | 11.01 | 0.1748 ± 20 | 2604 ± 19 |
| | 0.14 | 24 | 641 | 106 | 0.0490 | 0.446 | 10.81 | 0.1759 ± 18 | 2614 ± 17 |
| 30-2 rim | 0.38 | 89 | 795 | 89 | 0.0326 | 0.469 | 11.14 | 0.1721 ± 17 | 2578 ± 16 |
| | 0.14 | 32 | 779 | 84 | 0.0333 | 0.464 | 11.05 | 0.1726 ± 16 | 2583 ± 16 |
| 34-1 core | 0.43 | 82 | 663 | 116 | 0.0485 | 0.567 | 11.17 | 0.1734 ± 20 | 2590 ± 19 |
| | 0.25 | 48 | 656 | 121 | 0.0509 | 0.466 | 11.07 | 0.1724 ± 20 | 2582 ± 20 |
| 34-2 rim | 0.23 | 70 | 1,080 | 133 | 0.0335 | 0.452 | 10.58 | 0.1713 ± 15 | 2570 ± 14 |
| | 0.11 | 36 | 1,111 | 135 | 0.0344 | 0.455 | 10.75 | 0.1712 ± 15 | 2570 ± 15 |

[1] f% = % of $^{206}$Pb which is attributed to common Pb

5. The oldest zircon population is from the bulk sample 104055. This sample was from a heavy mineral concentrate that was sampled from the mill, and it is necessary to confirm that all the analyzed zircons originated from the pegmatite.

Figure 11 shows SHRIMP data from this study on a plot of $^{208}$Pb/$^{206}$Pb vs. $^{207}$Pb/$^{206}$Pb age. The data for zircons from the Millstream Dam granitoid have significantly higher $^{208}$Pb/$^{206}$Pb than the pegmatite zircons, nominally reflecting the distinctively low Th/U in the specialized pegmatitic melt. Zircons from the Logue Brook granitoid (Compston et al., 1986) have $^{208}$Pb/$^{206}$Pb ratios similar to the Millstream Dam granitoid, although the range of data is greater and includes one zircon with $^{208}$Pb/$^{206}$Pb that overlaps the Greenbushes pegmatite data. However, Compston et al. (1986; Fig. 4) noted from a concordia plot of $^{208}$Pb/$^{232}$U vs. $^{207}$Pb/$^{235}$U that zircon data from the Logue Brook granitoid showed a dramatic decoupling of $^{208}$Pb and $^{206}$Pb, with preferential $^{208}$Pb loss from many of the analyzed zircons. This is particularly apparent in data with a high common Pb correction (i.e., f > 1%), the more discordant data, and data with young $^{207}$Pb/$^{206}$Pb ages reflecting modern and old Pb loss, respectively. Similar plots for the zircon data of this study (not shown) showed little decoupling of $^{208}$Pb from $^{206}$Pb for the Millstream Dam granitoid data. However, the Greenbushes pegmatite data are similar to the Logue Brook granitoid, with the majority of data from zircons in all three pegmatite samples showing discordance on a $^{208}$Pb/$^{232}$U vs. $^{207}$Pb/$^{235}$U concordia diagram, mostly with preferential $^{208}$Pb loss with respect to $^{206}$Pb. This observation cannot be adequately explained from the available data and adds uncertainty to the interpretation of zircon $^{208}$Pb/$^{206}$Pb ratios for determining primary Th/U characteristics. Nonetheless, the consistently low $^{208}$Pb/$^{206}$Pb ratio in all zircons from the three pegmatite samples probably reflects an unusually low Th/U for the pegmatitic melt and was probably imparted to all pegmatitic zircons. It is noteworthy that the zircon data show no systematic difference in $^{208}$Pb/$^{232}$U vs. $^{207}$Pb/$^{235}$U concordia characteristics between the three pegmatite samples and, together with ore-related mineral inclusions in some of the zircons from the bulk sample 104055, support a pegmatitic origin for the zircons in this sample.

The Greenbushes pegmatite data are plotted on a concordia diagram in Figure 12A. A concordant to slightly reverse discordant, group of data with high $^{207}$Pb/$^{206}$Pb (from the bulk sample 104055) give statistically indistinguishable $^{207}$Pb/$^{206}$Pb ratios corresponding to a pooled age of 2527 ± 2 Ma ($2\sigma$); this is taken as the age of intrusion and the initial crystallization of the Greenbushes pegmatite. This age is significantly younger than the muscovite Rb/Sr model age (de Laeter and Blockley, 1978), which may have been affected by Rb loss during later deformation and metamorphism. The slight reverse discordance of some of the data is interpreted to result from Pb gain from uraninite inclusions, which occur in many of the zircons from the Greenbushes pegmatite. The remaining zircon data fall along a poorly defined Pb loss chord, which if taken through the 2527 Ma upper intercept has a lower intercept of 1100 ± 220 Ma. The veracity of this age is not known, although it does correspond to the age of a major resetting event which affected all Archean pegmatites within the Donnybrook-Bridgetown shear zone (McNaughton et al., 1988). A notable feature of the concordant to near-concordant data with $^{207}$Pb/$^{206}$Pb ages > 2400 Ma (Fig. 12B) is the presence in all three samples of zircons with $^{207}$Pb/$^{206}$Pb ages of 2430 to 2440 Ma. Six of the 14 analyzed grains show $^{207}$Pb/$^{206}$Pb ages in this range, and two of these grains (grain 11 in 104088 and grain 2 in 104055; Table 5) have areas of the grain which are significantly older. From the limited data it is not clear whether this group represents zircon growth at this time due to regional metamorphism, contact metamorphism due to dolerite dike intrusion, a prolonged crystallization history of the pegmatite or, less likely, an artifact of the complex geologic history of the pegmatite.

In the light of the SHRIMP data, the temporal history of the pegmatite includes emplacement at 2527 Ma, with continuing or episodic crystallization or hydrothermal remo-

TABLE 5. Zircon Results from the Greenbushes Pegmatite Samples

| Grain spot | f%[1] | $^{204}$Pb (ppb) | U (ppm) | Th (ppm) | $^{208}$Pb/$^{206}$Pb | $^{206}$Pb/$^{238}$U | $^{207}$Pb/$^{235}$U | $^{207}$Pb/$^{206}$Pb (± 2$\sigma$) | Minimum age (Ma ± 2$\sigma$) |
|---|---|---|---|---|---|---|---|---|---|
| Sample 104047 | | | | | | | | | |
| 2-1 | 0.05 | 31 | 2,105 | 42 | 0.0047 | 0.450 | 9.84 | 0.1588 ± 9 | 2443 ± 10 |
| | 0.07 | 40 | 2,119 | 43 | 0.0044 | 0.440 | 9.63 | 0.1588 ± 9 | 2443 ± 10 |
| 2-2 | 0.19 | 114 | 2,371 | 86 | 0.0058 | 0.417 | 9.05 | 0.1575 ± 9 | 2429 ± 12 |
| | 0.12 | 69 | 2,274 | 78 | 0.0051 | 0.424 | 9.21 | 0.1574 ± 9 | 2428 ± 12 |
| 5-1 | 0.31 | 105 | 1,383 | 45 | 0.0042 | 0.400 | 8.69 | 0.1575 ± 13 | 2429 ± 14 |
| | 0.10 | 36 | 1,457 | 47 | 0.0087 | 0.395 | 8.57 | 0.1573 ± 12 | 2427 ± 13 |
| Sample 104088 | | | | | | | | | |
| 1-1 | 1.10 | 166 | 1,076 | 16 | 0.0162 | 0.232 | 3.56 | 0.1111 ± 25 | 1817 ± 41 |
| | 0.41 | 51 | 979 | 16 | 0.0100 | 0.210 | 3.16 | 0.1092 ± 22 | 1786 ± 37 |
| 1-2 | 0.83 | 139 | 1,217 | 13 | 0.0000 | 0.229 | 2.89 | 0.0916 ± 21 | 1460 ± 45 |
| | 0.38 | 66 | 1,218 | 14 | 0.0044 | 0.238 | 3.01 | 0.0917 ± 18 | 1461 ± 37 |
| 2-1 | 0.18 | 136 | 2,642 | 28 | 0.0026 | 0.469 | 10.64 | 0.1646 ± 10 | 2504 ± 11 |
| | 0.12 | 93 | 2,738 | 29 | 0.0022 | 0.471 | 10.73 | 0.1652 ± 10 | 2509 ± 10 |
| 2-2 | 0.21 | 180 | 2,988 | 31 | 0.0025 | 0.470 | 10.59 | 0.1633 ± 9 | 2491 ± 10 |
| | 0.12 | 107 | 3,105 | 32 | 0.0043 | 0.473 | 10.71 | 0.1641 ± 9 | 2499 ± 10 |
| 8-1 | 0.52 | 145 | 1,433 | 33 | 0.0039 | 0.326 | 6.01 | 0.1338 ± 16 | 2149 ± 22 |
| | 0.33 | 91 | 1,415 | 33 | 0.0064 | 0.329 | 6.11 | 0.1345 ± 16 | 2158 ± 21 |
| 8-2 | 0.48 | 145 | 1,725 | 85 | 0.0049 | 0.293 | 4.23 | 0.1048 ± 15 | 1711 ± 27 |
| | 0.36 | 103 | 1,698 | 31 | 0.0020 | 0.281 | 4.16 | 0.1075 ± 16 | 1758 ± 28 |
| 9-1 | 0.40 | 89 | 840 | 8 | 0.0008 | 0.446 | 9.78 | 0.1590 ± 18 | 2445 ± 13 |
| | 0.23 | 52 | 846 | 8 | 0.0014 | 0.444 | 9.69 | 0.1582 ± 17 | 2437 ± 19 |
| 9-2 | 0.40 | 102 | 1,013 | 11 | 0.0004 | 0.425 | 9.19 | 0.1568 ± 17 | 2421 ± 18 |
| | 0.19 | 50 | 1,038 | 11 | 0.0020 | 0.425 | 9.25 | 0.1578 ± 16 | 2433 ± 18 |
| 9-3 | 0.80 | 156 | 1,415 | 9 | 0.0000 | 0.231 | 3.43 | 0.1076 ± 21 | 1759 ± 36 |
| | 0.34 | 65 | 1,341 | 10 | 0.0029 | 0.240 | 3.66 | 0.1107 ± 18 | 1811 ± 30 |
| 11-1 | 0.19 | 131 | 2,918 | 47 | 0.0037 | 0.398 | 8.61 | 0.1569 ± 9 | 2423 ± 10 |
| | 0.12 | 79 | 2,872 | 54 | 0.0054 | 0.397 | 8.48 | 0.1550 ± 9 | 2402 ± 10 |
| 11-2 | 0.15 | 103 | 2,542 | 41 | 0.0057 | 0.442 | 9.98 | 0.1637 ± 9 | 2494 ± 9 |
| | 0.11 | 75 | 2,572 | 42 | 0.0059 | 0.445 | 10.01 | 0.1633 ± 9 | 2490 ± 9 |
| 11-3 | 0.31 | 187 | 2,489 | 43 | 0.0085 | 0.403 | 8.75 | 0.1576 ± 11 | 2430 ± 12 |
| | 0.23 | 140 | 2,577 | 45 | 0.0093 | 0.396 | 8.59 | 0.1574 ± 11 | 2428 ± 12 |
| 15-1 | 0.21 | 210 | 4,064 | 121 | 0.0072 | 0.402 | 8.51 | 0.1535 ± 9 | 2385 ± 10 |
| | 0.14 | 139 | 3,719 | 95 | 0.0092 | 0.433 | 9.43 | 0.1579 ± 10 | 2434 ± 11 |
| Sample 104055 | | | | | | | | | |
| 1-1 | 0.19 | 202 | 3,614 | 86 | 0.0016 | 0.488 | 11.18 | 0.1662 ± 7 | 2520 ± 7 |
| | 0.17 | 177 | 3,671 | 88 | 0.0019 | 0.466 | 10.70 | 0.1665 ± 8 | 2522 ± 7 |
| 1-2 | 0.16 | 163 | 3,401 | 61 | 0.0033 | 0.507 | 11.71 | 0.1677 ± 8 | 2535 ± 8 |
| | 0.15 | 163 | 3,677 | 67 | 0.0025 | 0.501 | 11.54 | 0.1669 ± 8 | 2527 ± 8 |
| 1-3 | 0.11 | 212 | 6,198 | 146 | 0.0054 | 0.513 | 11.73 | 0.1658 ± 6 | 2515 ± 5 |
| | 0.10 | 196 | 6,358 | 154 | 0.0052 | 0.504 | 11.59 | 0.1668 ± 6 | 2526 ± 6 |
| 1-4 | 0.16 | 112 | 2,593 | 44 | 0.0050 | 0.457 | 10.59 | 0.1682 ± 10 | 2539 ± 9 |
| | 0.07 | 52 | 2,599 | 45 | 0.0050 | 0.465 | 10.75 | 0.1676 ± 9 | 2534 ± 9 |
| 1-5 | 0.06 | 90 | 5,273 | 119 | 0.0067 | 0.512 | 11.88 | 0.1683 ± 6 | 2540 ± 5 |
| | 0.03 | 50 | 5,315 | 120 | 0.0066 | 0.514 | 11.91 | 0.1681 ± 6 | 2539 ± 6 |
| 2-1 | 0.21 | 236 | 3,797 | 57 | 0.0007 | 0.508 | 11.59 | 0.1655 ± 7 | 2513 ± 7 |
| | 0.20 | 226 | 3,980 | 59 | 0.0006 | 0.482 | 11.10 | 0.1669 ± 8 | 2527 ± 8 |
| 2-2 | 0.48 | 230 | 1,796 | 19 | 0.0158 | 0.450 | 9.74 | 0.1571 ± 16 | 2425 ± 18 |
| | 0.40 | 195 | 1,888 | 20 | 0.0076 | 0.438 | 9.59 | 0.1588 ± 12 | 2443 ± 13 |
| 2-3 | 0.77 | 209 | 1,136 | 11 | −0.0085 | 0.397 | 8.66 | 0.1584 ± 18 | 2439 ± 20 |
| | 0.89 | 249 | 1,211 | 12 | −0.0142 | 0.384 | 8.16 | 0.1542 ± 19 | 2393 ± 21 |
| 2-4 | 0.32 | 165 | 2,075 | 20 | 0.0170 | 0.412 | 9.04 | 0.1590 ± 13 | 2445 ± 14 |
| | 0.10 | 49 | 2,012 | 19 | 0.0151 | 0.411 | 9.30 | 0.1642 ± 12 | 2499 ± 12 |
| 4-1 | 0.79 | 245 | 1,551 | 18 | −0.0053 | 0.333 | 6.99 | 0.1521 ± 18 | 2369 ± 20 |
| | 0.66 | 198 | 1,562 | 18 | −0.0063 | 0.320 | 6.63 | 0.1505 ± 18 | 2351 ± 20 |
| 4-2 | 0.45 | 122 | 1,312 | 28 | 0.0036 | 0.344 | 6.81 | 0.1439 ± 18 | 2274 ± 21 |
| | 0.22 | 57 | 1,308 | 28 | 0.0047 | 0.336 | 6.54 | 0.1410 ± 16 | 2240 ± 20 |
| 5-1 | 0.71 | 249 | 1,642 | 27 | 0.0132 | 0.354 | 6.57 | 0.1349 ± 14 | 2163 ± 19 |
| | 0.61 | 207 | 1,674 | 28 | 0.0057 | 0.337 | 6.45 | 0.1390 ± 14 | 2215 ± 18 |
| 6-1 | 0.98 | 180 | 807 | 45 | −0.0132 | 0.378 | 7.49 | 0.1436 ± 23 | 2271 ± 28 |
| | 0.73 | 149 | 858 | 5 | −0.0116 | 0.395 | 8.02 | 0.1472 ± 22 | 2314 ± 26 |
| 6-2 | 0.37 | 53 | 551 | 4 | 0.0006 | 0.424 | 9.13 | 0.1564 ± 27 | 2417 ± 29 |
| | 0.27 | 38 | 564 | 4 | 0.0000 | 0.416 | 8.76 | 0.1526 ± 26 | 2375 ± 29 |

[1] f% = % of $^{206}$Pb which is attributed to common Pb

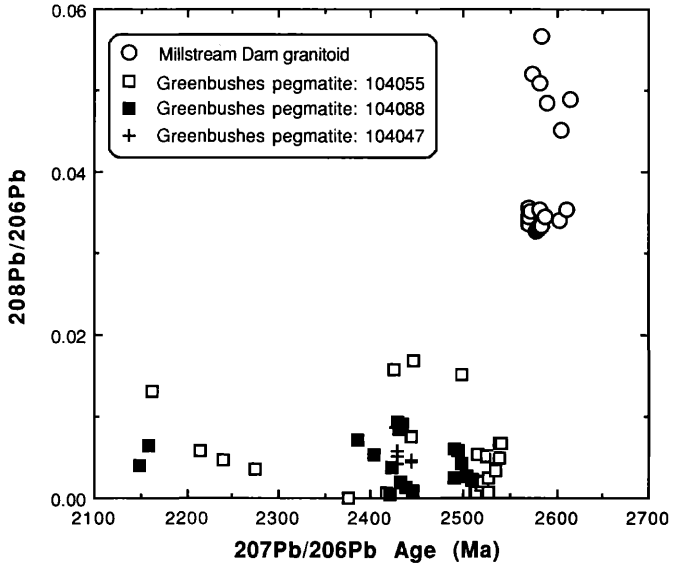


FIG. 11. Plot of zircon data with $^{207}Pb/^{206}Pb$ age > 2100 Ma from this study, on a $^{208}Pb/^{206}Pb$ vs. $^{207}Pb/^{206}Pb$ age diagram showing the consistently low $^{208}Pb/^{206}Pb$ of all pegmatite zircons relative to the Millstream Dam granitoid.

bilization to ca. 2430 Ma, possible resetting and Pb loss at 1100 Ma, and recent Pb loss. The exceptionally low $^{208}Pb/^{206}Pb$ and Th/U ratios of the zircons (Table 5) are anomalous for granitoids and probably reflect the highly specialized nature of the pegmatite melt (e.g., Černý, 1985), and they may afford a diagnostic signature indicating that all analyzed zircons were derived from the pegmatite (Fig. 11).

## Discussion and Conclusions

### *Geologic history of the pegmatite district*

Using published data and data from this study, it is possible to compile a detailed tectonic history for the pegmatite district (Fig. 13). The sequence of gneiss near Bridgetown (Fig. 1A) appears to be the oldest crustal component in the Greenbushes pegmatite district. Nd/Sm isotope studies indicate that this crustal material was separated from the mantle at ca. 3100 Ma (Fletcher et al., 1983), and as such it probably represents the earliest tectonothermal event in the area. This gneiss is similar in composition and character to orthogneisses intruded into the Donnybrook-Bridgetown shear zone (e.g., in the Millstream Dam granitoid or in the Logue Brook granitoid), suggesting that the precursors to these gneisses may have been felsic intrusive rocks. If so, then some earlier crustal material was present prior to the intrusion of these rocks at ca. 3100 Ma.

There is a record in the dioritic gneiss of an early noncoaxial deformation event, which occurred before the formation of the supracrustal sequence and intrusion of the younger granitoids at ca. 2600 Ma. It appears that this margin of the Yilgarn block was tectonically active for much of its Archean history and formed a major crustal suture along which later deformational events were concentrated. $D_1$ mylonitic fabrics indicate that a regional dextral transcurrent shear zone was active along the western margin of the craton between ca. 3100 and 2600 Ma.

The supracrustal sequences in the Greenbushes pegmatite district formed parallel to the trend of the Donnybrook-Bridgetown shear zone between ca. 2600 and 3100 Ma. An age of ca. 2800 Ma derived from granofels elsewhere in the western gneiss terrane (Rosman et al., 1980; see McNaughton and Dahl, 1987) suggests that these supracrustal sequences formed at a similar time. The lack of $D_1$ deformational structures and the presence of $D_2$ mylonitic fabrics indicate that this sequence formed after the deformation of the dioritic gneiss but parallel to a similar crustal structure.

Regional $D_2$ sinistral shearing, metamorphism, and granitoid intrusion began by 2610 Ma with the initial intrusion of the Logue Brook granitoid and possibly an early phase of the Millstream Dam granitoid. The intrusion of granitoids continued until at least 2577 Ma with intrusion of the Cowan Brook and Millstream Dam granitoids and ended with the intrusion of the Greenbushes pegmatite at 2527 Ma in association with peak $M_2$ metamorphism and $D_2$ deformation. These ages of events are slightly younger than those of the Saddleback greenstone belt and other greenstone belts in the Yilgarn block (see McNaughton et al., 1990), suggesting that

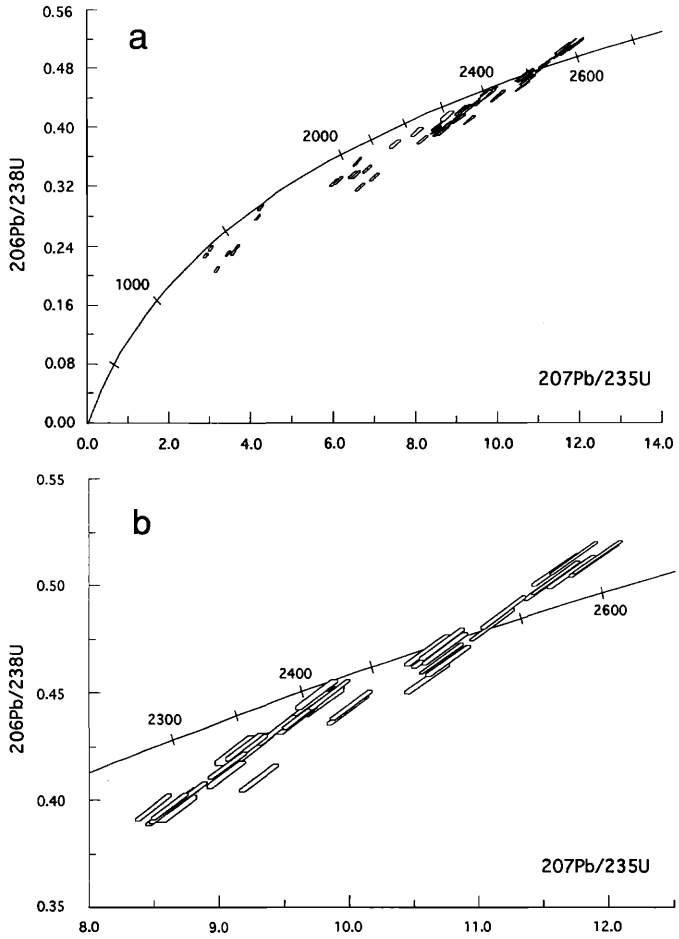


FIG. 12. Concordia plots of (a) all the zircon data from the Greenbushes pegmatite, and (b) the most concordant group with $^{207}Pb/^{206}Pb$ ages > 2400 Ma, which include analyses with high $^{207}Pb/^{206}Pb$ which are indistinguishable and correspond to an age of 2527 ± 2 Ma, and another grouping of analyses with $^{207}Pb/^{206}Pb$ ages of 2440 to 2430 Ma. Error boxes shown are 1$\sigma$.

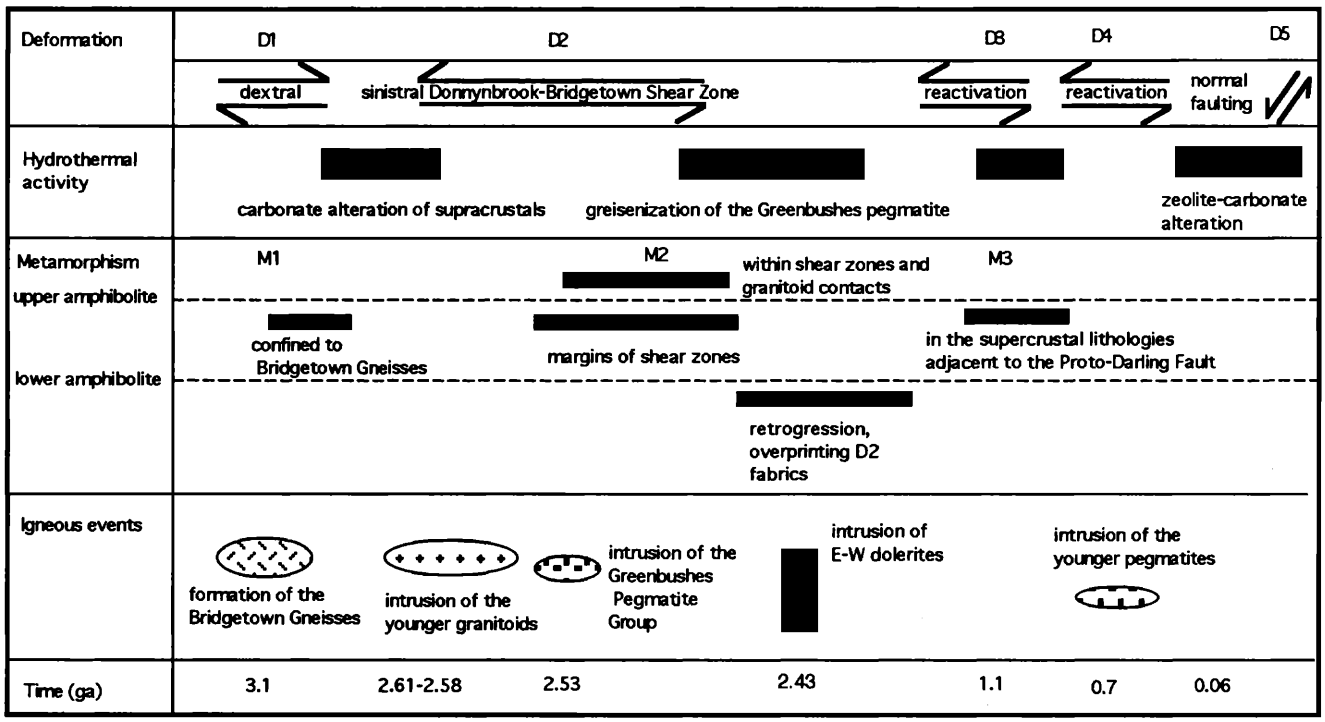


FIG. 13. Summary of the geologic history of the Greenbushes pegmatite district.

the younger tectonothermal processes were restricted to the craton margin toward the end of the Archean.

The intrusion of a regionally extensive east-west dolerite dike suite then occurred across the Yilgarn at ca. 2400 Ma (e.g., Jimberlana dike near Norseman at 2411 ± 55 Ma; Fletcher et al., 1987). The dolerite dikes intruded the pegmatite causing contact metamorphism and local remelting of the pegmatite. The intrusion of these dikes may have also caused hydrothermal alteration of the pegmatite along $D_2$ shear zones and the consequential remobilization of mainly tantalum mineralization and the growth of the 2430 to 2440 Ma zircon population represented in all pegmatite samples.

The resetting of the mineral Pb-Pb and zircon U-Pb data suggests that further deformation and metamorphism occurred between ca. 1300 and 1100 Ma due to reactivation along the major structure encompassing the Greenbushes pegmatite district (Partington et al., 1986, 1988, 1990b; McNaughton et al., 1988). These ages agree with ages derived for metamorphism, deformation, and granitoid emplacement in the Albany-Fraser province (Rosman et al., 1980; Fletcher et al., 1983, 1991; McNaughton and Dahl, 1987; Pidgeon, 1990). East-west Proterozoic foliation and aeromagnetic trends overprint the Archean trends to the south of the Balingup metamorphic belt (Fig. 1C), indicating that significant movement along the Donnybrook-Bridgetown shear zone had ceased except for minor $D_3$ movements at ca. 1100 Ma.

Further metamorphism, deformation, and pegmatite intrusion occurred between the Darling fault and the Donnybrook-Bridgetown shear zone (Fig. 1B). Aeromagnetic evidence and fabric trends shown in Figure 1C suggest the presence of a major shear zone, the precursor to the Darling fault (Harris, 1987), which was active toward the end of the Proterozoic (Kepert, 1985; Partington et al., 1986). This proto-Darling fault zone truncates and offsets the Proterozoic trends south of the Manjimup lineament in the Albany-Fraser province and is probably responsible for the sinistral offset of the Archean gneisses in the south of the Balingup metamorphic belt (Fig. 1D).

The last recognized metamorphic event in the district occurred at ca. 700 to 500 Ma and is marked by reactivation of sinistral shearing, metamorphism, and intrusion of the Ferndale pegmatite (Kepert, 1985) and Mullalyup pegmatite (Seet, 1986). These ages broadly correspond with other ages from the Western Australian Shield, Antartica, southern Africa, and India associated with a major Pan-African tectonothermal event prior to fragmentation of Gondwana (Windley, 1982). There is also evidence for widespread activity along the whole of the western margin of the Yilgarn block at this time in response to a major tectonothermal event.

### *Crystallization and mineralization history of the Greenbushes pegmatite*

Preliminary conclusions of the crystallization history of the pegmatite combining the paragenetic data from Paterson (1983) and Bettenay et al. (1985), structural data from Partington (1988), temperature data from Han (1991) and Han and Collins (1993) and age data from Partington (1988, 1990b) and this study are summarized in Figures 5 and 13. Crystallization of the pegmatite commenced with tourmaline in the albite zone and tourmaline zone at 890°C, followed by albite, cassiterite, and tantalite in the albite zones and tourmaline zones at 750°C. Zircons from these zones and this phase of crystallization gave the maximum recorded age of 2527 ± 2 Ma. This was followed by crystallization of spodu-

mene-quartz assemblages in the footwall lithium zone at a temperature of 770°C. Crystallization of the hanging-wall K feldspar zone was coeval or transitional with the hanging-wall lithium zone at 700° to 690°C.

Deformation and metamorphism were synchronous with the intrusion and crystallization of the pegmatite. This deformation caused fracturing of early formed minerals, which then became suitable sites for the second phase of mineralization and continuing crystallization of tourmaline, albite, muscovite, spodumene, and beryl at a temperature of 680°C. It is interpreted that a second episode of zircon growth occurred at this time along with cassiterite and microlite. The younger zircons (2.43–2.4 Ga) can either be interpreted to have formed as a result of hydrothermal crystallization of the pegmatite over a 90 m.y. time interval, or as a result of significant remelting and/or hydrothermal remobilization of the pegmatite during regional metamorphism or the intrusion of the east-west dolerite dike suite. The overlap of the younger zircon ages with the ages determined elsewhere in the Yilgarn craton for the intrusion of east-west dolerite dikes and the observation that many of the more economic Ta-bearing ore shoots are located in the vicinity of the dolerite dikes (e.g., Highway Shoot and Tantalite Corner) provide circumstantial evidence that dolerite intrusion and associated hydrothermal remobilization of pegmatite is the preferred interpretation of the younger zircon age. Because of the small number of zircon grains analyzed during this preliminary study further work is necessary. Finally, the third stage of mineralization occurred at a temperature of 620°C associated with greisenlike zones within $D_3$ shear zones which can be related to later $D_3$ deformation and metamorphism. This deformation and metamorphism affected the crosscutting Proterozoic dolerite dikes and is interpreted to have occurred at ca. 1100 Ma.

*Implications for the source of the Greenbushes pegmatite*

The source of pegmatitic melts is a controversial subject (Černý, 1982b). In many cases a genetic relationship can be inferred between pegmatites and parental granitoids. However, larger rare metal pegmatites commonly lie outside the influence of any major parental granitoid, and a hidden parental granitoid is usually invoked as a source for these rare metal pegmatites. Such a relationship has been suggested for the Greenbushes pegmatite (Blockley, 1980). None of the outcropping granitoids in the pegmatite district show evidence for specialization and were therefore not considered to be genetically related to the Greenbushes pegmatite (Table 1; Blockley, 1980). However, a highly fractionated apophysis from the nearby Wheatbelt batholith was invoked at depth to be parental to the Greenbushes pegmatite (Blockley, 1980). Considering the highly fractionated nature of the Greenbushes pegmatite, any parental granitoid would have to be up to several orders of magnitude larger than the pegmatite (e.g., by a factor of 70 for lithium pegmatites; Stewart, 1978). The Greenbushes pegmatite is a minimum size of 6 × 0.5 × 0.4 km (Hatcher and Elliot, 1986), although these are the present-day dimensions; considering the major alluvial deposits that are present, the pegmatite must have been considerably larger. Further, drilling has yet to define the base of the pegmatite, and the dimensions given by Hatcher and Elliot (1986) should be considered a minimum estimate. The present minimum volume of pegmatite is some 1.2 $km^3$, suggesting that a parental granitoid of >80 $km^3$ should exist at depth beneath the pegmatite.

Detailed gravity surveys available for the district discount any possibility for a major parental granitoid existing at depth in the vicinity of the pegmatite (Partington, 1988). The only body of granitoid large enough to be parental to the pegmatite is the nearby Wheatbelt batholith. Compston et al. (1986) dated a pluton of the Wheatbelt batholith, the Logue Brook granitoid, using the SHRIMP U/Pb zircon technique at 2612 ± 5 Ma, some 85 m.y. before the intrusion of the Greenbushes pegmatite at 2527 ± 2 Ma. Similar ages were derived from the granitoid plutons in the vicinity of the pegmatite, confirming that granitoid intrusion throughout the district occurred at least 85 to 50 m.y. before pegmatite intrusion. The age dating provides additional evidence for the mineralogical and geochemical studies that the simple relationship between a parental granitoid and a rare metal pegmatite as described by Černý (1982a and b) does not exist in the Greenbushes pegmatite district.

## Acknowledgments

Research was carried out as part of a Ph.D. project at the University of Western Australia by G.A.P. and was funded by a Commonwealth postgraduate research award with financial assistance from Greenbushes Tin NL. We are indebted to David Groves, without whom this project would never have been conceived, for his ideas and patience, Leigh Bettenay for his supervision during the project, and Bill Compston (Australian National University) for access and advice on the SHRIMP ion microprobe. We are grateful to the staff of Greenbushes Tin NL, including Roger Thompson, Mike Hatcher, John Davis, and Geoff Glynik, for logistical support and helpful discussions during visits to Greenbushes. We are also grateful to Helen Williams for her patience and careful drafting work and to Colin Hughes and Franz Hock for photographic work. The isotope facilities used during this project are supported by the Australian National University, University of Western Australia, and Curtin University of Technology.

## REFERENCES

Bettenay, L.F., Groves, D.I., and Partington, G.A., 1985, Development of exploration concepts for Sn-Ta pegmatites: Use of host-rock associations and alteration halos: Western Australian Mineral and Petroleum Research Institute Report, v. 13, 171 p.

Bettenay, L.F., Partington, G.A., Groves, D.I., and Paterson, C., 1988, Nature and emplacement of the giant rare-metal Greenbushes pegmatite, at Greenbushes, Western Australia: International Association on the Genesis of Ore Deposits Quadrennial Symposium, 7th, Proceedings, p. 401–408

Blockley, J.G., 1980, The tin deposits of Western Australia: Western Australia Geological Survey of Mineral Research Bulletin 12, 184 p.

Černý, P., 1982a, Anatomy and classification of granitic pegmatites: Mineralogical Association of Canada Short Course Handbook, v. 8, p. 1–40.

—— 1982b, Petrogenesis of granitic pegmatites: Mineralogical Association of Canada Short Course Handbook, v. 8, p. 405–462.

—— 1985, Some recent advances in the mineralogy and geochemistry of Nb and Ta in rare-element granitic pegmatites: Bulletin de Mineralogie, v. 108, p. 499–532.

Compston, W., Williams, I.S., and Meyer, C., 1984, U-Pb geochronology of zircons from lunar breccia 73217 using a sensitive high mass-resolution ion microprobe: Journal of Geophysical Research, v. 89, p. B525-B534.

Compston W., Williams, I.S., and McCulloch, M.T., 1986, Contrasting zircon

U-Pb and model Sm-Nd ages for the Archaean Logue Brook Granite: Australian Journal of Earth Sciences, v. 33, p. 193–200.

Cumming, G.L., and Richards, J.R., 1975, Ore lead isotope ratios in a continuously changing earth: Earth and Planetary Science Letters, v. 28, p. 155–171.

de Laeter, J.R., and Blockley, J.G., 1978, Age of a tin-bearing pegmatite at Greenbushes: Western Australia Geological Survey Annual Report, 1977, p. 48–50.

Fletcher, I.R., Wilde, S.A., Libby, W.G., and Rosman, K.J.R., 1983, Sm-Nd model ages across the margins of the Archean Yilgarn block, Western Australia—II: Southwest transect into the Proterozoic Albany-Fraser province: Geological Society of Australia Journal, v. 30, p. 333–340.

Fletcher, I.R., Libby, W.G., and Rosman, K.J.R., 1987, Sm-Nd dating of the 2411 Ma Jimberlana dyke, Yilgarn block, Western Australia: Australian Journal of Earth Sciences, v. 34, p. 523–525.

Fletcher, I.R., Myers, J.S., and Ahmat, A.L., 1991, Isotopic evidence on the age and origin of the Fraser Complex, Western Australia: Chemical Geology, v. 87, p. 197–216.

Gee, R.D., Baxter, J.L., Wilde, S.A., and Williams, I.R., 1981, Crustal development in the Archean Yilgarn block, Western Australia: Geological Society of Australia Special Publications, v. 7, p. 43–56.

Han, T., 1991, Evolution of a magmatic-hydrothermal fluid during crystallization of the Greenbushes pegmatite: Unpublished M.Sc. thesis, Perth, Curtin University of Technology, 246 p.

Han, T., and Collins, P.L.F., 1993, Rare metal mineralisation during magmatic-hydrothermal transition in the Greenbushes pegmatite, Western Australia [abs.]: Geological Society of Australia Abstracts, no. 34, p. 24–25.

Harris, L.B., 1987, A tectonic framework for the Western Australian Shield and its significance to gold mineralization: A personal view: University of Western Australia Geology Department and University Extension Pub. 11, p. 1–27.

Hartely, M.R., 1982, Metasomatism between the Greenbushes pegmatite and mafic rocks: Unpublished B.Sc. thesis, Perth, University of Western Australia, 45 p.

Hatcher, M.I., and Elliot, A., 1986, Greenbushes—a new world resource of lithium: Industrial Minerals International Congress, 7th, Proceedings, p. 217–232.

Jaffey, A.H., Flynn, K.F., Glendenin, L.E., Bentley, W.C., and Essling, A.M., 1971, Precision measurements of half-lives of $^{235}U$ and $^{238}U$ [abs.]: Physics Review, v. C4, p. 1889.

Kepert, D., 1985, The structural environment and age of the Ferndale pegmatite: A re-evaluation of the tectonics of the Balingup metamorphic belt: Unpublished B.Sc. thesis, Perth, University of Western Australia, 71 p.

Koon, L.H., 1973, Geology and geochemistry of the Greenbushes pegmatite and its immediate country rocks: Unpublished B.Sc. thesis, Perth, University of Western Australia, 60 p.

Ludwig, K.R., 1980, Calculation of uncertainties of U-Pb isotope data: Earth and Planetary Science Letters, v. 46, p. 212–220.

London, D., and Burt, D.M., 1982, Lithium minerals: Mineralogical Association of Canada Short Course Handbook, v. 8, p. 99–122.

McNaughton, N.J., and Bickle, M.J., 1987, K-feldspar Pb-Pb isotope systematics of Archaean post-kinematic granitoid intrusions of the Diemals area, central Yilgarn block, Western Australia: Chemical Geology, v. 66, p. 193–208.

McNaughton, N.J., and Dahl, N., 1987, A geochronological framework for gold mineralization in the Yilgarn block: University of Western Australia Geology Department and University Extension Pub. 11, p. 29–50.

McNaughton, N.J., Partington, G.A., Seet, L.H., and Kepert, D.A., 1988, Craton margin tectonics and the origin of Sn-Ta pegmatites in the southwest Yilgarn block—the Pb isotope approach [abs.]: Geological Society of Australia Abstracts, no. 21, p. 274–275.

McNaughton, N.J., Cassidy, K.F., Groves, D.I., and Perring, C.S., 1990, Constraints on genesis of primary gold deposits: Timing of mineralization: University of Western Australia Geology Department and University Extension Pub. 20, p. 221–225.

Moorbath, S.M., and Taylor, P.N., 1981, Isotopic evidence for continental growth in the Precambrian: Developments in Precambrian Geology, v. 4, p. 491–525.

Norton, J.J., 1983, Sequence of mineral assemblages in differentiated granitic pegmatites: ECONOMIC GEOLOGY, v. 78, p. 854–874.

Page, L.R., Adams, J.W., Erickson, M.P., Hall, W.E., Hanley, J.B., Joralemon, P., Norton, J.J., Pray, L.C., Steven, T. A., Stoll, W.C., and Stopper, R.F., 1953, Pegmatite investigations 1942–45 Black Hills, South Dakota: U.S. Geological Survey Professorial Paper 247, 228 p.

Partington, G.A. 1986, The tectonic controls on the intrusion of specialized pegmatites in the Greenbushes pegmatite district, Western Australia [abs.]: Bureau of Mineral Resources Record 1986/10, p. 53–54.

—— 1988, The geochronology, tectonic environment and structural controls on intrusion of the giant rare-metal pegmatite at Greenbushes, Western Australia: Unpublished Ph.D. thesis, Perth, University of Western Australia, 120 p.

—— 1990a, Environment and structural controls on the intrusion of the giant rare metal Greenbushes pegmatite, Western Australia: ECONOMIC GEOLOGY, v. 85, p. 437–456.

—— 1990b, Geology of the southwest Yilgarn and Greenbushes Pegmatite Group: University of Western Australia Geology Department and University Extension Pub. 21, p. 123–144.

Partington, G.A., McNaughton, N.J., Kepert, D.A., Compston, W., and Williams, I.S., 1986, Geochronology of the Balingup metamorphic belt: Constraints on the temporal evolution of the Greenbushes pegmatite district [abs.]: Australian Bureau of Mineral Resources Record 1986/10, p. 55–56.

Paterson, C., 1983, A petrogenetic study of zoning in the Greenbushes pegmatite, Western Australia: Unpublished B.Sc. thesis, Perth, University of Western Australia, 50 p.

Pidgeon, R.T., 1990, Timing of plutonism in the Albany-Fraser mobile belt, southwestern Australia: Precambrian Research, v. 47, p. 157–167.

Ramsay, J.G., and Huber, M.I., 1983, The techniques of modern structural geology, vol. 1: Folds and fractures: London, Academic Press, 700 p.

Rosman, K.J.R., Wilde, S.A., Libby, W.G., and de Laeter, J.R., 1980, Rb-Sr dating of granitic rocks in the Pemberton area: Western Australia Geological Survey Annual Report, 1979, p. 97–100.

Seet, L.H., 1986, Pegmatite K-feldspars as guides to rare-metal mineralization and crustal evolution in the Balingup metamorphic belt, Western Australia: Unpublished B.Sc. thesis, Perth, University of Western Australia, 87 p.

SOG, 1991, Gwalia Consolidated Ltd. Annual Report 1991: Annual report to the Australian Stock Exchange, 63 p.

Stewart, D.B., 1978, Petrogenesis of lithium-rich pegmatites: American Mineralogist, v. 63, p. 970–980.

Tatsumoto, M., Knite, R. J., and Allegre, C. J., 1973, Time differences in the formation of meteorites as determined from the ratio of lead-207 to lead-206: Science, v. 180, p. 1279–1283.

Wilde, S.A., and Walker, I.W., 1979, Explanatory notes on the Collie 1:250,000 geological sheet, Western Australia: Western Australia Geological Survey Record 11, 81 p.

Williams, I.S., Compston, W., Black, L.P., Ireland, T.R., and Foster, J.J., 1984, Unsupported radiogenic Pb in zircon: A cause of anomalously high Pb-Pb, U-Pb and Th-Pb ages: Contributions to Mineralogy and Petrology, v. 88, p. 322–327.

Windley, B.F., 1982, The evolving continents: New York, John Wiley and Sons, 385 p.

York, D., 1969, Least squares fitting of a straight line with correlated errors: Earth and Planetary Science Letters, v. 5, p. 320–324.